

# Dilation and confining stresses in shear thickening of dense suspensions

Eric Brown and Heinrich M. Jaeger

*The James Franck Institute, University of Chicago, Chicago, IL 60637*

(Dated: September 11, 2010)

Many densely packed suspensions and colloids exhibit a dramatic behavior known as Discontinuous Shear Thickening in which the viscosity jumps apparently dramatically and reversibly at a certain shear rate. We performed rheometry and video microscopy measurements on a variety of densely packed suspensions to determine the mechanism for this behavior. We distinguish Discontinuous Shear Thickening from inertial effects by showing that the latter are characterized by a Reynolds number but are only found up to packing fractions around 0.4, while the former are significant only at higher packing fractions. If the suspended particles are heavy enough to settle we find the onset of shear thickening  $\tau_{min}$  corresponds to a hydrostatic pressure which is required to shear the particles against gravity and friction. Combined with previous results for colloids this suggests that generally  $\tau_{min}$  corresponds to the stress required to shear neighboring particles apart. Shear profiles and normal stress measurements indicate that stresses are transmitted through frictional rather than viscous interactions implying the particles remain in contact via force chains while sheared. Above  $\tau_{min}$ , dilation is observed as an apparent roughness of the surface, indicating the viscosity jump coincides with a change in the boundary condition. The upper stress boundary  $\tau_{max}$  of the shear thickening regime is shown to roughly match the ratio of surface tension divided by a radius of curvature on the order of the particle size. This scaling suggests the viscosity jump comes from the confining stress due to capillary forces as the liquid-air interface at the boundary is deformed by dilation. A similar change in boundary conditions happens without shear when the packing fraction is increased beyond the jamming transition where a yield stress on the scale of  $\tau_{max}$  develops as a result of particles penetrating the liquid-air interface. We generalize this shear thickening mechanism to other sources of a confining stress by showing that when instead the suspensions are confined by solid walls and have no liquid-air interface, then  $\tau_{max}$  is set by the stiffness of the wall. With these new scaling laws, we can delineate the shear thickening regime in a phase diagram that encompasses the scalings found not only for suspensions but also colloids with Brownian and electrostatic interactions.

PACS numbers: 83.85.Cg, 83.80.Hj, 83.60.Rs

## I. INTRODUCTION

Shear thickening is a category of non-Newtonian fluid behavior in which the viscosity  $\eta$  defined by  $\eta = \tau/\dot{\gamma}$  increases as a function of shear rate  $\dot{\gamma}$  or shear stress  $\tau$  over some parameter range. A particularly dramatic form, often called Discontinuous Shear Thickening [1–24], occurs in many densely packed suspensions such as cornstarch in water. These suspensions feel like a thin liquid when stirred slowly, but feel very thick and can even crack like a solid when stirred harder, and become thin again when the stress is removed. Such materials are of practical interest for their properties as dampeners and shock absorbers [25–27]. While there are various models for shear thickening and some milder types of shear thickening are well-understood as inertial effects [28, 29], they have not been very successful at describing the dramatic effects found in dense suspensions. Our goal with this paper is to describe a universal mechanism behind Discontinuous Shear Thickening in enough detail to determine which suspension properties are relevant and if other systems besides suspensions can exhibit the phenomenon. Given properties of a suspension or colloid such as packing fraction, particle size, surface tension, zeta potential, we should be able to predict if it will shear thicken, and if so in what parameter range. We will use

a combination of rheometry and video microscopy measurements to answer the above questions. Our approach differs from previous work in that we consider a granular point of view in addition to the traditional hydrodynamic approach.

The dramatic shear thickening observed in dense suspensions by Refs. [1–24] can be characterized by a few universal properties (see Fig. 4 for an example). Thus we find it convenient to define the phenomenon of Discontinuous Shear Thickening based on these properties and to distinguish this behavior from other types of shear thickening:

1. Stress scales: The boundaries of the shear thickening regime are simply described in terms of stress scales (rather than shear rate) which are mostly independent of packing fraction and liquid viscosity [8, 11, 18, 22]. Consequently, the onset shear rate varies with packing fraction and liquid viscosity since suspension viscosities increase with both parameters [33]. Shear thinning or Newtonian behavior is found at lower stresses before the onset of shear thickening at a stress  $\tau_{min}$ . Above the upper stress boundary of the shear thickening regime  $\tau_{max}$ , shear thinning is usually found up to the point where the suspension cracks or spills.
2. Diverging slope: The term ‘Discontinuous’ refers to

the apparent discontinuous jump in  $\tau(\dot{\gamma})$  of orders of magnitude at the onset of shear thickening. This jump is only observed at very high particle packing fractions around 0.5 for nearly spherical particles. The slope of  $\tau(\dot{\gamma})$  is only very steep over a few percent range in packing fraction, lessening significantly at lower packing fractions [11, 17, 22]. The packing fraction dependence of the slope of  $\tau(\dot{\gamma})$  can be characterized as a power law diverging at a packing fraction  $\phi_c$  [22]. Above this packing fraction the system is jammed meaning it will not flow for applied stresses below a non-zero yield stress of scale  $\tau_j$ .

3. **Reversibility:** The Discontinuous Shear Thickening described above is reversible, meaning viscosity curves show similar shear thickening whether they are measured with increasing or decreasing stress histories. Some examples of dramatic shear thickening have been found to be irreversible because of chemical-attraction-induced aggregation [30, 31] or occur only in transient behavior [32], and will not be considered here as they may be different phenomena.

The remainder of this paper is organized as follows. In Sec. II we review the literature on shear thickening and which aspects of the existing models can be applied specifically to Discontinuous Shear Thickening. In Sec. III we describe the rheometry techniques and suspensions used in our experiments. In Sec. IV we show viscosity curves for shear thickening suspensions at different packing fractions and liquid viscosities. With this we can compare them to hydrodynamic inertial scalings which we find to be applicable only to lower packing fractions than where dramatic shear thickening effects are found. In Sec. V we show measurements of  $\tau_{min}$  for different particle sizes and liquid densities to quantify the effect of gravity on  $\tau_{min}$ . In Sec. VI we show shear profile measurements with different liquid densities to see the role of gravity in the shape of the shear profile and how it changes in different rheological regimes. In Sec. VII we show results of measurements made with a fixed normal force on the sample and to test the connection between shear and normal stresses in shear thickening. From this we find a global constitutive relation that is frictional rather than viscous. In Sec. VIII we use images of the surface of the suspensions at rest for different packing fractions to show the onset of a yield stress coincides with a visible change in the boundary as particles penetrate the liquid-air interface. We also show that a similar visible change occurs with shear due to dilation. In Sec. IX we propose that this boundary condition results in a confining stress due to surface tension which can set the scale of the stress response to shear. We then show that comparisons of the measured stress and dilation are consistent with this model, and that this confining stress scale agrees with measurements of the upper bound of the shear thickening regime  $\tau_{max}$  for different suspen-

sions over a wide range of particle sizes. In Sec. X we generalize this result to other types of confining stress by showing measurements from a rheometer with solid walls instead of a liquid-air interface and show that  $\tau_{max}$  is set by the stiffness of the wall. In Sec. XI we discuss our results in terms of dominant stress scales of the system, and combine our results with other scalings found in different parameter regimes to delineate typical boundaries of the shear thickening regime for suspensions and colloids. We conclude with a summary of the general conditions for Discontinuous Shear Thickening.

## II. BACKGROUND

Because of the vast amounts of literature referring to different phenomena and mechanisms which all fall under the category of shear thickening, we first carry out a review of the literature try to clarify which results in the literature apply to Discontinuous Shear Thickening. We will suggest based on the literature that hydrodynamic models which have been successful for describing other types of shear thickening have been insufficient for describing Discontinuous Shear Thickening. Rather, there is significant evidence supporting the significance of dilation and normal forces which suggests we should additionally consider a granular point of view.

In contrast to the Discontinuous Shear Thickening described above, there are other types of shear thickening with different characteristics. One common type of shear thickening can be described in hydrodynamic terms where the onset occurs when inertial momentum transport overcomes diffusive momentum transport, analogous to high Reynolds number flow. For colloids it is described in terms of a Peclet number [29, 34], and for non-Brownian suspensions in terms of a Bagnold number [28]. Each of these characterized by an onset shear rate in contrast to an onset stress for Discontinuous Shear Thickening. For inertial scalings  $\tau(\dot{\gamma}) \propto \dot{\gamma}^2$  in the limit of high shear rates. Because of the less steep  $\tau(\dot{\gamma})$ , such shear thickening is often called Continuous Shear Thickening. If the stress/shear-rate relation in the shear thickening regime is expressed  $\tau \sim \dot{\gamma}^\alpha$ , we can thus identify shear thickening in a suspension as Discontinuous if an  $\alpha > 2$  can be observed at high packing fractions and  $\alpha$  increases with packing fraction, and Continuous if  $\alpha \leq 2$  at all packing fractions. Continuous Shear Thickening can be observed even at very low packing fractions and has a much weaker packing fraction dependence than Discontinuous Shear Thickening. We will show an example of this in Sec. IV.

Because of the qualitative differences between Discontinuous and Continuous Shear Thickening, we suspect they are different phenomena with different mechanisms, and remain focused here on Discontinuous Shear Thickening [76]. For this reason, we will not assume any results that apply to Continuous Shear Thickening also apply to Discontinuous shear thickening. This is a different ap-

proach than much of the literature which attempts to unify all types of shear thickening by a single hydrodynamic mechanism [11, 33, 35]. The typical approach has been to start with the hydrodynamic models of Continuous Shear Thickening which are well-understood at low packing fractions [29], and extend them to higher packing fractions. The expectation is that at higher packing fractions, hydrodynamically-induced clusters of particles form in which nearby particles act transiently as a solid cluster when they get so close to each other that the lubrication drag force between them blows up [33, 36]. While this mechanism seems plausible, so far the calculations have failed to reproduce viscosity curves similar to experimental measurements of Discontinuous Shear Thickening.

One prediction that was made from these calculations is the stress at the onset of shear thickening. In early models for Brownian-motion dominated colloids the onset was described by a critical Peclet number  $Pe = 6\pi\eta\dot{\gamma}a^3/kT$  for a particle size  $a$  and thermal energy  $kT$ . Shear thickening is expected to occur for  $Pe \gtrsim 100$  as the shear stress overcomes thermal diffusion of the particles [29, 36]. This model has been successful at calculating the onset of shear thickening for both Continuous and Discontinuous Shear Thickening when written in terms of a stress scale  $\tau = kT/6\pi a^3$  independent of the liquid viscosity [12, 34]. For colloids where repulsions from a zeta potential are dominant the above model had to be modified [11]. In that case, the particular scaling found was a stress characterizing electrostatic particle interactions. While the forces were calculated at a distance corresponding to an effective hydrodynamic radius, calculating at a different radius would only change a scale factor of order 1, and since the model was an order-of-magnitude calculation, it would likely have resulted in just as good a match with the data. The modifications to the hydrodynamic model required to fit it to the data resulted in completely eliminating any dependence on hydrodynamic parameters such as viscosity or shear rate. The resulting stress scale is not specific to hydrodynamic mechanisms, as any type of forces transferred through a continuum system can be expressed in terms of a stress. With several relevant forces in colloids and suspensions, each of which could be dominant in different cases, a variety of different scalings for the onset have been found. The common trend is that the onset can be described more simply in terms of a stress scale (rather than a shear rate) independent of packing fraction and set by some dominant force in the system. Depending on the parameter range, this dominant force could be Brownian motion [29], zeta potential [11], particle-liquid surface tension [23], induced dipole attractions [23], or steric repulsion [70]. Notably, in each case hydrodynamic terms such as shear rate and viscosity were absent from the modified scalings which match the experiments, so this suggests inertia or hydrodynamics-based models are not necessary to determine the onset of Discontinuous Shear Thickening as initially envisioned by the Peclet number

scalings.

To understand the mechanism for shear thickening we focus on the scaling laws for the stress scales  $\tau_{min}$  and  $\tau_{max}$  to gain insight into the relevant physical mechanisms. We will revisit the subject of the onset stress in Sec. V to come up with a universal description that encompasses all of these scalings without the need to refer to a hydrodynamic model. Another limitation of purely hydrodynamic models is that they do not have a mechanism to account for the upper bound of the shear thickening regime  $\tau_{max}$ . It has been suggested that this could be fixed by accounting for the finite stiffness of particles which allows for particle deformation [35], but again this is not inherently a hydrodynamic correction. We will address the issue of the upper stress boundary in Sec. IX.

While we could simply approach the problem in terms of dominant stress scales as a modification of the hydrodynamic model as many others have done [10, 11, 30, 34], we will show that starting with a hydrodynamic model is not necessary and the significance of the stress scales holds independent of the hydrodynamic models. A major advantage of this approach is that different mechanisms such as interparticle forces, gravity, and surface tension can be simply expressed in terms of stress scales which can be compared to the measured stress scales without the need to reference a base model. Another good reason to try to understand Discontinuous Shear Thickening independent from the hydrodynamic models is that some features of the rheology that suggest a granular rather than hydrodynamic perspective on the system.

Granular materials can have properties of solid, liquids, or gases under different conditions [37]. For example, randomly packed particles at high enough packing fractions cannot shear or compress because geometric constraints force them to be in contact, so they behave like a solid. At lower packing fraction the particles are able to move around each other freely in a liquid-like state. The transition between these two regimes is sharp and is known as the jamming transition [38]. For shear thickening suspensions, the divergence of the slope of  $\tau(\dot{\gamma})$  at a critical packing fraction  $\phi_c$  was found to correspond to the jamming transition [22].

Forces tend to be transmitted through granular packings along concentrated paths called force chains [39] such that the distribution of forces is characterized by an exponential tail [40]. Simulations of shear thickening colloids have similarly found contact networks between particles with an exponential distribution of forces [41].

Sheared granular flows are often characterized by shear bands, in which the shear flow is mostly localized, typically near the moving boundary such that the velocity profile is exponential for spherical particles [42] as opposed to the linear shear profile typical of Newtonian flows. We will show shear profile measurements in Sec. VI.

A feature of granular shear flows with special relevance to shear thickening is dilation [43, 44]. When a granular packing is sheared, the particles have to go around each

other so the packing dilates, taking up more space than it does at rest. It has long been known that dilation occurs along with Discontinuous Shear Thickening [1]. In fact, in some of the literature ‘dilatancy’ has used as a synonym for shear thickening [5]. Especially important in understanding this relationship was a paper by Metzner and Whitlock [1]. They showed that for  $\text{TiO}_2$  suspensions of 0.2-1  $\mu\text{m}$  particles, dilation initiated at stresses close to the onset of shear thickening for a range of packing fractions. However, suspensions of 28-100  $\mu\text{m}$  glass spheres in sucrose solutions were found to dilate but not shear thicken in a Couette cell [1], showing that dilation was not always equivalent to shear thickening. For 40+ years following this result, many of the major papers on shear thickening dropped the focus on dilation in favor of hydrodynamic descriptions [4, 11, 33]. However, there is another possible interpretation of Ref. [1]. Metzner and Whitlock confirmed for several suspensions that the onset was the same for both dilation and shear thickening, as had been seen in many previous results. Thus suggested at least a strong connection between dilation and shear thickening. Inductively those results suggested that dilation was necessary but not sufficient for Discontinuous Shear Thickening. More recent results have shown one such condition, that shear thickening can be hidden by a yield stress or other shear thinning effect [23]. Recent measurements have systematically shown that such large, heavy particles as the glass beads used by Ref. [1] will jam in a Couette cell because they settle under gravity, resulting in a yield stress [45], explaining why shear thickening was not observed for the settling particles of Ref. [1]. It has only been in the last 10 years that dilation has become prominent again in the shear thickening literature [10, 15, 16, 21]. However, a mechanism by which dilation leads to a dramatic increase in stress has yet to be explained. This is the subject of Sections VIII, IX, and X.

When dilation of granular shear flows is prevented by confinement, shear is instead accompanied by normal forces against the walls [43, 44]. For Discontinuous Shear Thickening suspensions normal forces are usually found to be positive, meaning the sample is pushing against the rheometer plate [15, 16, 21, 24, 46]. This direction is consistent with dilation arguments. It was proposed by Ref. [21] that shear thickening cannot occur if the normal stress is taken away. We will investigate this in Sec. VII.

### III. MATERIALS AND METHODS

#### A. Tools

Measurements were performed with an Anton Paar Physica MCR 301 rheometer which measures the torque  $T$  required to shear a sample at a tool rotation rate  $\omega$ . Most measurements were done in a parallel plate setup where normal forces could be measured. This geometry is shown in Fig. 1a and characterized by the plate radius

$R = 12.5$  (or 25) mm and gap size  $d$  between the plates. A few measurements were done with a cylindrical cup-and-bob (Couette) geometry in which the environment is better-controlled. The tool surfaces are smooth stainless steel. The viscosity, indicating the mechanical resistance to shear, is defined as  $\eta \equiv \tau/\dot{\gamma}$  in a steady state. For the parallel plate setup, for example, we represent the global shear stress by

$$\tau = \frac{2T}{\pi R^3} \quad (1)$$

and the shear rate by

$$\dot{\gamma} = \frac{R\omega}{d}. \quad (2)$$

These standard coefficients give the local stress at the edge of the plate in the case of a Newtonian shear profile, but may overestimate it by as much as 25% for different shear profiles. The reported global shear stress and shear rate values are meant to characterize the mechanical response in a way that is independent of system size so it can be compared to other physically relevant stress scales.

In the parallel plate measurements, the upward force on the rheometer tool is measured and the mean normal stress  $\tau_N$  is obtained by dividing this normal force by the plate cross-sectional area. The standard deviation of the force measured during a static measurement over 10 s intervals with or without sample is  $6 \times 10^{-4}$  N, giving a relative uncertainty of 0.3 Pa (1.2 Pa) for a 50 mm (25 mm) diameter plate. The standard deviation of the average force measured after calibration with no sample is  $4 \times 10^{-3}$  N, giving an absolute uncertainty of 2 Pa (8 Pa) for a 50 mm (25 mm) diameter plate.

The Anton Paar MCR 301 rheometer has special settings for normal force control measurements. Our reported measurements were done with value of ‘normal force hysteresis’ set to 0.001 N. This value controls how much the normal force can deviate from the set value before the plate moves in response, although in practice the plate tends not to move until the normal force deviation exceeds about 0.01 N (20 Pa for the 25 mm plate). The ‘normal force dynamics’ value was set to 0% (default). This value controls acceleration of the gap size in the feedback loop. This setting corresponds to the most reproducible steady state gap sizes, and the slowest acceleration of the gap so it is responds slowly to variations in the normal force.

The typical parallel plate setup is shown in Fig. 1a, in which the suspension is held in place between the parallel plates by surface tension at the liquid-air interface around the side. Because we saw that particles could penetrate the liquid-air interface (see Sec. VIII) which we suspected could modify the stresses on the suspension from the interfacial tension, we desired a different boundary condition with a hard wall for some experiments. Thus we machined an aluminum cylindrical cup

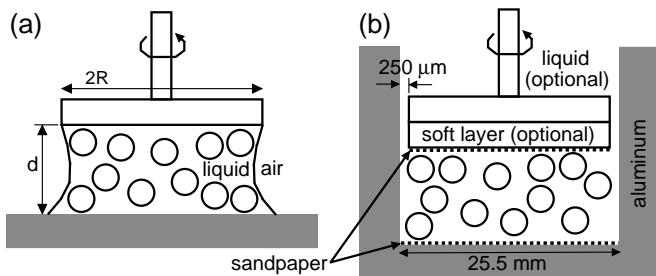


FIG. 1: (a) A standard parallel plate rheometer setup. The suspension is confined between the plates by the surface tension of the suspending liquid. (b) A modified parallel plate setup with solid walls around the sample. In this setup the use of a suspending liquid is optional, and the wall stiffness can be modified by inserting layers of different material between the suspension and plate.

with diameter 25.5 mm as shown in Fig. 1b. The cup fits around the tool with a gap small enough to prevent 500  $\mu\text{m}$  diameter particles from slipping through but large enough to allow the tool to rotate without friction. This cup confined the particles to the volume beneath the plate, while the liquid could be filled to a higher level or omitted altogether so there is no liquid-air interface for particles to penetrate. The plates were covered with sandpaper sheets with a grit size of 100  $\mu\text{m}$  to avoid slip with dry grains. In some cases we inserted a soft layer in between the top plate and sandpaper to modify the compliance of the wall.

## B. Suspensions

We studied suspensions with a variety of particle types and liquids to show that shear thickening is a universal phenomenon.

As a prototypical shear thickener we used cornstarch obtained from Argo. Cornstarch particles have a mean diameter of 14  $\mu\text{m}$  and density of 1.59 g/mL based on buoyancy in CsCl solutions. They are very hydrophilic and hard – with a compression modulus on the order of  $10^{10}$  Pa – at room temperature. At higher temperatures the polymers that compose cornstarch particles can gel. To compare suspensions with different liquid viscosities, we suspended cornstarch in either a mixture of 61.5% water and 38.5% CsCl by weight with a viscosity of 1 mPa·s and density of 1.41 g/mL or a mixture of 73.5% glycerol 13.0% water, and 13.5% CsCl by weight with a viscosity of 80 mPa·s and density of 1.34 g/mL. For such small particles, the settling time is several hours even without density matching.

For a series of suspensions in which we vary particle size but have otherwise constant materials we used soda-lime glass spheres with a density of 2.46 g/mL. We obtained particles with nominal diameter ranges of 3-10  $\mu\text{m}$ , 10-25  $\mu\text{m}$ , and 15-40  $\mu\text{m}$  from Corpuscular, 45-63  $\mu\text{m}$ , 75-104  $\mu\text{m}$  (referred to as 100  $\mu\text{m}$ ), 177-250  $\mu\text{m}$ , and

400-595  $\mu\text{m}$  from MoSci (Class IV), and 1120-1350  $\mu\text{m}$  and 1900-2100  $\mu\text{m}$ . For polydisperse suspensions, no observable effect on the onset stress  $\tau_{min}$  has been found since data can be collapsed based on the geometric mean particle size [11], thus we will compare particle distributions only by their mean diameter. The glass spheres were dispersed in various liquids, including water or mineral oil with a viscosity of 58 mPa·s and density of 0.87 g/mL.

For visualization purposes we used two types of opaque particles. The first, referred to as  $\text{ZrO}_2$ , were spheres obtained from Glen Mills consisting of 69%  $\text{ZrO}_2$  and 31%  $\text{SiO}_2$ . They have a nominal diameter range of 100-200  $\mu\text{m}$  and a density of 3.8g/mL. These particles were dispersed in the same mineral oil used for the glass particles. For experiments with density matched suspensions, we used polyethylene spheres obtained from Cospheric. These particles have a nominal diameter range of 125-150  $\mu\text{m}$  and density of 1.01 g/mL. They were dispersed in silicone oil AR 20 with a nominal density of 1.01 g/mL and viscosity of 20 mPa·s. When varying the temperature of the suspension, we found that the settling time was minimized at 19° C from which we estimated a density difference of order  $10^{-4}$  g/mL.

We also include some summary data for particles fabricated into different shapes from polyethylene glycol (PEG) (see Ref. [23] for details) suspended in liquid PEG-250, and 100  $\mu\text{m}$  spheres made of polystyrene dimethyl ether suspended in PEG.

## C. Measurement procedure

Measurements were made with the bottom plate temperature controlled at 20° C. The room humidity ranged from 22% to 38%, although during individual experiments the humidity was constant. This affects the amount of evaporation/adsorption of water from/to suspensions which can result in an apparent time dependence in measurements due to the sensitive packing fraction dependence of shear thickening suspensions [22]. To minimize evaporation or adsorption, we used a solvent trap when the suspending liquid was water which enclosed the sample and a small amount of air around it by an extra layer of liquid. The enclosed air equilibrated with the sample to prevent further changes to the suspension.

Packing fractions  $\phi$  are measured as the volume of solid particles over the total volume of solids and liquid. While this packing fraction is fixed during measurements, the packing fraction in space may decrease slightly during measurements as the grain packing dilates and liquid moves inward. Above the jamming transition, the packing fraction in space may be less than the packing fraction in liquid if air bubbles become trapped in the interior. Humidity also has a large effect on the amount of water adsorbed onto dry grains open to the atmosphere, especially cornstarch which is hygroscopic

so that 10-20% of the weight of the ‘dry’ powder is from water. Comparison of density measurement techniques suggest that cornstarch is porous or that it may absorb CsCl, thus we report mass fractions for cornstarch rather than volumetric packing fractions. For the humidity conditions and CsCl concentrations used, the jamming transition occurs at about the same mass fraction in cornstarch suspensions as the packing fraction for solid spheres ( $\phi_c = 0.56$  for cornstarch in water,  $\phi_c = 0.58$  for cornstarch in the glycerol-water mixture, and  $\phi_c = 0.57$  for solid spheres). Thus the mass fractions for cornstarch suspensions roughly correspond to packing fractions for sphere suspensions under our experimental conditions, but we note this is just a coincidence and comparing packing fractions of cornstarch suspensions under different conditions is not trivial.

The gap size  $d$  for parallel plate measurements was usually chosen to about 1 mm, large enough to avoid finite-size effects on the viscosity for particles around 100  $\mu\text{m}$  in diameter [24]. We have measured bulk shear thickening with both rough and smooth plates and did not find any difference in the shear thickening due to the plate surface. To directly measure slip, we used video microscopy to observe the shear profile at the outer edge of the plate. The results of these measurements are shown in Sec. VI. Spillage of suspension out of the region between the plates during measurements is a concern, so we visually confirmed that the suspensions do not spill for all reported measurements. Spillage was often the limiting factor in the maximum stress or shear rate applied for our measurements.

Viscosity curves were measured by first pre-shearing immediately before measurements for at least 100 seconds at shear rates above the shear thickening regime where the steady state flow is fully mobilized, then ramping the control parameter (shear stress or rate) down then up to obtain hysteresis loops. To ensure that we obtain steady state viscosity curves, the measurement ramp should be long enough that the size of the hysteresis loop is equal to that of the infinite duration limit. To check this, we show data in Fig. 2 for a sample of 100  $\mu\text{m}$  glass spheres in mineral oil at  $\phi = 0.56$ , which is a stable sample over long time periods because the oil does not evaporate. Viscosity curves shown were taken first with a decreasing stress ramp then an increasing stress ramp for several different ramp durations. Since the control is a logarithmic ramp in stress over 4 decades, the measurement duration is specified in terms of duration per decade of stress. The hysteresis effect is characterized by a geometric mean of viscosity ratios  $\langle \eta_-(\tau)/\eta_+(\tau) \rangle_g$  averaged over the stress range of 0.1 to 8 Pa in the shear thickening regime where  $\eta_-$  and  $\eta_+$  are viscosity for decreasing and increasing stress ramps, respectively, and  $\langle \dots \rangle_g$  indicates a geometric mean. The hysteresis initially decreases with increasing measurement duration, then levels off for long measurements indicating a steady state limit. The initial duration-dependent behavior is characteristic of a transient relaxation, and the crossover between the regimes

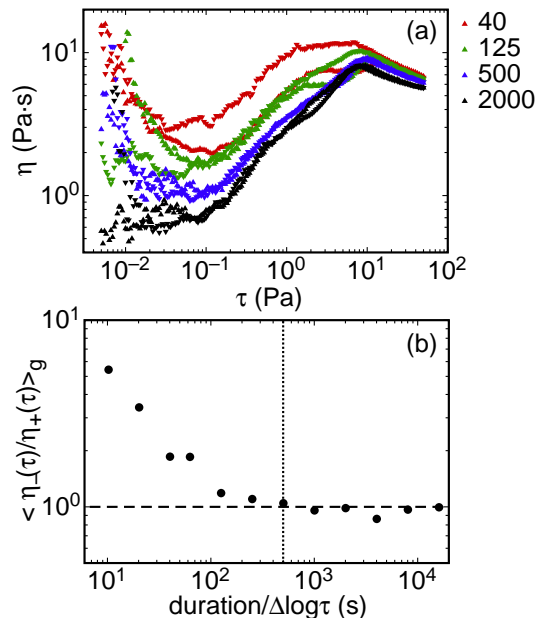


FIG. 2: (a) Apparent viscosity curves for 100  $\mu\text{m}$  glass spheres in mineral oil taken at different measurement durations to show hysteresis loops. Up-pointing triangles correspond to increasing stress ramps, while down-pointing triangles correspond to decreasing stress ramps. Ramp durations per decade of the stress ramp are given in the key. (b) Characterization of the hysteresis by a geometric mean of viscosity ratio between the decreasing and increasing ramps for different ramp durations per decade of stress. Dashed line: a ratio of 1 between increasing and decreasing ramps corresponding to no hysteresis. Dotted line: ramp rate used for later steady state measurements

indicates the characteristic timescale for the sample to reach steady state. The leveling off of the stress ratio at a value of 1 suggests that in this case there is not a true hysteresis effect. At packing fractions very close to the jamming transition we sometimes find some non-zero hysteresis loop even for very long measurements, such that different steady states can be reached dependent on the shear history. The steady state viscosity curves we report are generally in the long-duration regime where the hysteresis loop has converged to a value near 1, for this sample we typically use a control ramp rate of 500 s per decade of stress. For each steady state measurement, we ramped the control parameter down then up at least once, but we show only one set of curves for brevity if they were all identical within typical variations of 10-20% from run to run.

#### IV. INERTIAL SCALINGS

In this section we show some examples of viscosity curves for suspensions at different packing fractions. While there are already many examples of the strong packing fraction dependence, here we vary the liquid vis-

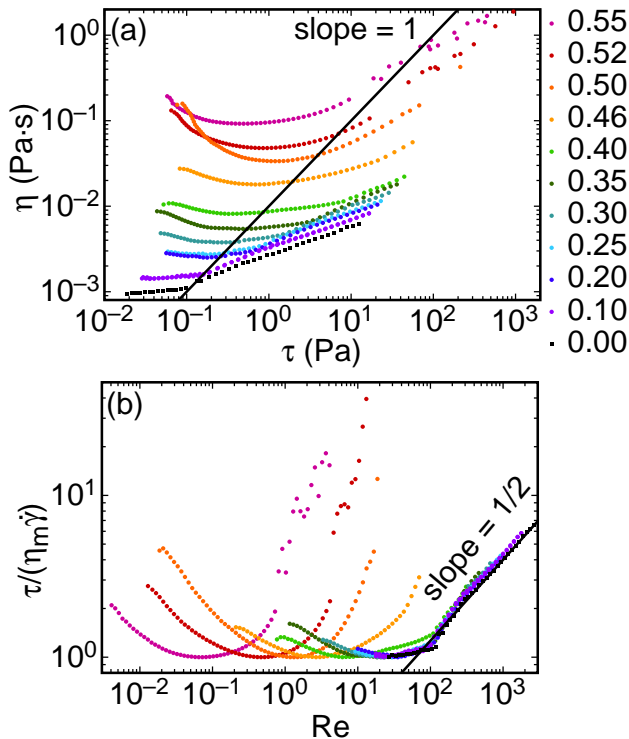


FIG. 3: (a) Viscosity vs. stress curves for suspensions of cornstarch in water. Mass fractions  $\phi_m$  are shown in the key. The solid line corresponds to a constant shear rate. (b) A rescaling of the data as  $\tau/\eta_m\dot{\gamma}$  vs. Reynolds number  $Re = \rho\dot{\gamma}d^2/\eta_m$  which should result in a data collapse for hydrodynamic flows. The line corresponds to a scaling  $\tau \sim \dot{\gamma}^{3/2}$  in the range  $100 \lesssim Re \lesssim 3000$  which is typical.

cosity and the packing fraction from near the jamming transition all the way down to zero to connect to hydrodynamic scalings that apply for suspensions at low concentrations and to quantify the importance of inertia in shear thickening.

We first show measurements of cornstarch suspended in water. These measurements were made with the Couette geometry. Viscosity is plotted vs. shear stress for several packing fractions in Fig. 3a. Apparent shear thickening is seen as regions with a positive slope of the viscosity curve for all packing fractions. For pure liquids this can be quantified in terms of a dimensionless Reynolds number, which represents a ratio of inertial to viscous forces. This Reynolds number is usually of the form  $\rho d^2\dot{\gamma}/\eta_l$  for pure liquids where  $\rho$  and  $\eta_l$  are the density and dynamic viscosity of the liquid, respectively. For the pure liquid the transition from a Stokes regime with a constant viscosity to an inertia-dominated regime with apparent shear thickening depends on shear rate. However, we find that the transition to shear thickening for suspensions does not occur at the same shear rate for different packing fractions; specifically for low packing fractions the onset shear rate increases with packing fraction. The contribution of viscous forces to the vis-

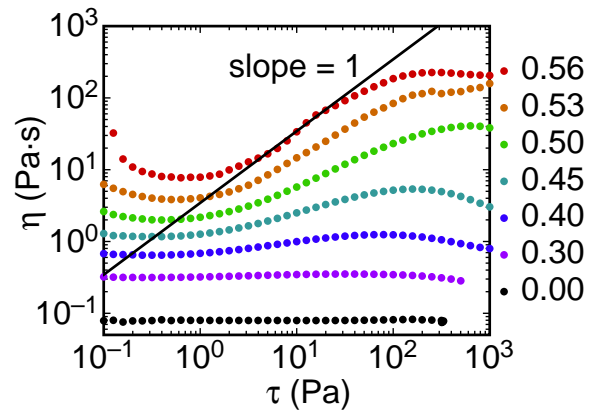


FIG. 4: Viscosity curves for cornstarch in a glycerol-water mixture in which the Reynolds number remains small. Mass fractions  $\phi_m$  are shown in the key. The solid line of slope 1 corresponds to a constant shear rate and the steepest possible steady state viscosity curve.

cosity of dense suspensions is much higher than the pure liquid even in the Stokes regime [33], so the viscous term in the denominator of the Reynolds number should be modified for suspensions. For the Stokes flow contribution to suspension viscosity we do not take the zero shear rate limit of the viscosity since in this limit suspensions rheology can be dominated by non-viscous particle interactions [5, 11, 23, 29], which results in shear thinning at low shear rates. Rather, we take as our best estimate the minimum suspension viscosity  $\eta_m$  at the onset of shear thickening for each packing fraction. Our suspension Reynolds number is then  $Re = \rho\dot{\gamma}d^2/\eta_m$ .

In Fig. 3b we plot the shear stress normalized by  $\eta_m\dot{\gamma}$  corresponding to the Stokes flow contribution to the stress vs. our suspension Reynolds number  $Re$  in Fig. 3. With this normalization, data for any Newtonian fluid should collapse onto the same curve. We find that the lower mass fractions  $\phi_m \lesssim 0.4$  tend to collapse onto a similar curve. The approximate scaling  $\tau \sim \dot{\gamma}^{3/2}$  for  $100 \lesssim Re \lesssim 3000$  is typical for inertial hydrodynamic flows in this range of  $Re$  [53]. The scaling collapse for  $\phi_m \lesssim 0.4$  suggests that in this regime the suspension behaves like a Newtonian fluid in that the mechanical viscosity is dominated by viscous hydrodynamics and inertia is responsible for the weak shear thickening at high  $Re$ . In contrast, for  $\phi_m \gtrsim 0.4$  the normalized viscosity curves deviate significantly from this scaling with steeper shear thickening which onsets at much lower values of  $Re$ , rather the onset appears to be set by a stress scale instead[77]. This suggests that inertia is negligible in the regime where shear thickening becomes more dramatic. This does not necessarily imply that viscous forces are dominant in the system, as we will show in Sec. VII that friction is a dominant mechanism of stress transfer at high packing fractions.

The scaling seen in Fig. 3 suggests two competing mechanisms for shear thickening. To obtain a system

where the Reynolds number remains low in the Discontinuous Shear Thickening stress range even at low packing fractions, a liquid of higher viscosity can be used. To see Discontinuous Shear Thickening without inertial effects we suspended cornstarch in a glycerol-water mixture. The measured viscosity of this liquid mixture is 80 times that of water. The viscosity curves vs. stress for different packing fractions can be seen in Fig. 4. Comparing with the data for cornstarch in water in Fig. 3, we can see that there is similar strong shear thickening at high packing fractions, but no apparent shear thickening at low packing fractions. At the same stress, the Reynolds number is lower by about a factor of  $\eta_l^2 \approx 600$  for the glycerol suspension, thus  $Re < 100$  and inertial effects remain negligible in the stress range of Discontinuous Shear Thickening even in the limit of zero packing fraction. We can see the remaining shear thickening uncontaminated by inertial effects is now very weak at  $\phi_m = 0.40$ , and is almost imperceptible at  $\phi_m = 0.30$ . This is a typical example of Discontinuous Shear Thickening, in which the region with positive slope of  $\eta(\tau)$  occurs in a stress range that is nearly independent of packing fraction, and this slope increases with packing fraction, approaching  $\eta \sim \tau$  (solid line in Fig. 4) corresponding to a discontinuous stress/shear-rate relation as the jamming transition is approached. The bounds of the shear thickening regime are characterized on the low end by  $\tau_{min}$  defined as the onset of a positive slope of  $\eta(\tau)$ , and on the high end by  $\tau_{max}$  defined as the transition from positive to negative slope. Because of fluctuations and variations from run to run of around 10-20% we do not count any features smaller than that threshold as distinct rheological regimes.

There are several other dimensionless numbers that have been used to describe inertial effects in particulate flows. In particular, they often replace the system size  $d$  with the particle size  $a$ , for example a Bagnold number [28]. The distinction between the two types of scalings can be made with the data at zero packing fraction which has the system size scale of  $d$  but no particle length scale. Since the cornstarch in water data for  $\phi_m \lesssim 0.4$  including  $\phi_m = 0$  collapse based on a Reynolds number scaling in terms of  $d$ , the system size should be taken as the relevant length scale as is typical in pure fluids. Since the Reynolds number scaling comes from pure liquids, it appears that the global steady state viscosity of suspensions can be described by Newtonian hydrodynamics up to packing fractions as high as 0.4, and possibly higher in larger systems where inertial effects are stronger. At higher packing fractions, strong shear thickening can be seen at lower shear rates which may overwhelm inertial effects. We can qualitatively distinguish high- $Re$  flow from Discontinuous Shear Thickening because of the packing fraction, shear rate, liquid viscosity, and gap size dependence of high- $Re$  flows differs from that of Discontinuous Shear Thickening, and the steepest possible scaling for inertial flows is  $\tau \sim \dot{\gamma}^2$  in the limit of large shear rates [28]. Since the focus of this paper is

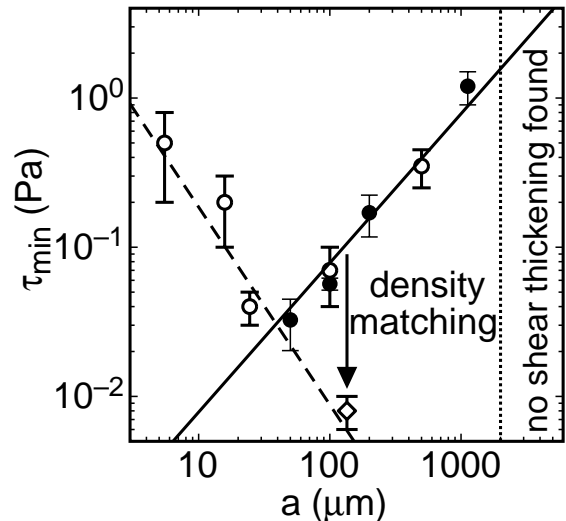


FIG. 5: The stress at the onset of shear thickening  $\tau_m$  for glass spheres of different diameters  $a$  in mineral oil (solid circles,  $\Delta\rho = 1.58$  g/mL) or water (open circles,  $\Delta\rho = 1.46$  g/mL). Open diamonds: polyethylene in silicone oil ( $\Delta\rho \approx 0.0001$  g/mL). The solid line is the shear stress required to lift particles off the top layer of the packing against friction and gravity  $\mu_{eff}\Delta\rho ga/15.3$ . Dashed line: representative curve for data where gravity is not the dominant interparticle interaction. Dotted line: bound above which larger particles did not have any shear thickening regime.

on Discontinuous Shear Thickening, all of the following data will be in the high packing fraction regime with  $\phi > 0.4$  and for  $Re < 100$  to avoid mixing with apparent shear thickening from inertial effects.

## V. GRAVITY AND THE ONSET STRESS

Suspensions and colloids occupy a region of phase space where many physical forces may be relevant; these include Brownian motion, gravity, surface tension, and electrostatics. The result has been different scaling laws for the onset of shear thickening in different parameter regimes where one of these forces is dominant [11, 12, 18, 23, 29, 36, 70]. Here we address the case of a gravity-dominated regime, which is not as well-characterized as the other regimes. A study of the effects of gravity on the onset stress will make it possible to further generalize the conditions for the onset of shear thickening beyond what is already known for suspensions with a yield stress [23].

We measured steady state viscosity curves for a series of suspensions of glass spheres ( $\rho = 2.46$  g/mL) with diameters ranging from 6 to 2000  $\mu\text{m}$  in diameter in either mineral oil ( $\rho = 0.88$  g/mL) or water ( $\rho = 1.00$  g/mL) at packing fractions ranging from 0.50 to 0.58. These particles are large enough to settle over time since the glass is much denser than the liquids. In each case, the major

features were qualitatively similar to Fig. 4, with increasingly steep slopes at higher packing fractions and shear thickening occurring in a relatively fixed stress range. We obtain mean values of  $\tau_{min}$ , corresponding to the onset of a positive slope of  $\eta(\tau)$ , for each suspension over a range of packing fractions close to but below  $\phi_c$ . The mean values of  $\tau_{min}$  for each particle size are plotted in Fig. 5. It is clearly seen that there are at least two distinct scaling regimes, which cross at a minimum near a particle size of  $50 \mu\text{m}$  is where the two scalings meet.

For the largest particles with  $a \geq 500 \mu\text{m}$ , the suspensions would not remain confined between the rheometer plates with a vertical boundary because the particles are so heavy that they can no longer be confined by surface tension. Since this condition is set by a comparison between gravitational and surface tension forces, it is no surprise that this occurs on the order of the capillary length, or  $\sim 1 \text{ mm}$ . We could still make measurements with some sample extended outside the area between the plates to obtain the scales of  $\tau_{min}$  and  $\tau_{max}$ . For the largest glass beads with a diameter of  $2000 \mu\text{m}$ , we found no shear thickening regime. The significance of this maximum particle size for shear thickening will be discussed in Sec XI.

For smaller particles with  $a \leq 50 \mu\text{m}$  that approach the colloidal regime, interparticle interactions from various sources including electrostatics and Brownian motion tend to become larger relative to gravity and can affect the onset stress. For example, a high particle-liquid surface tension can result in an effective attraction between particles which can form force chains that span the system and jam it, resulting in a yield stress and shear thinning even at low packing fractions which can hide shear thickening [23]. Specifically for this measurement series, with glass beads  $50 \mu\text{m}$  and larger, the particles will disperse well and shear thicken in either oil or water. However, the  $6 \mu\text{m}$  glass particles are effectively hydrophilic so in oil they have a significant yield stress and shear thickening was not observed at all. We will revisit the issue of other scaling regimes for the onset in Sec. XI.

To understand the scaling of  $\tau_{min}$  for the larger particles with  $a \geq 50 \mu\text{m}$ , here we analyze the effects of gravity on non-Brownian suspensions. In the absence of shear, gravity results in particles settling and resting on the bottom plate. The measured stress would come only from shear of the thin fluid layer on top of the settled particles. The drag force from the shear in the liquid layer above the particles can start to move the upper layer of particles if it exceeds the static frictional force between particles under gravity. In a parallel plate geometry, the horizontal cross-section has a uniform area so since forces must be balanced the shear stress  $\tau$  must be on average independent of height. As an estimate for the drag force on the top layer of particles, we use drag force on a sphere sitting on a flat surface is  $2.55\pi\tau a^2$  [52]. The frictional force is  $\pi\mu_{eff}\Delta\rho ga^3/6$  for an effective static coefficient of friction  $\mu_{eff}$ , density difference between the particles and liquid  $\Delta\rho$ , and acceleration of

gravity  $g$ . Since the particle is sitting on a pile of beads instead of a flat surface, the effective friction is enhanced by geometry because of the need for the spheres to rise over the particles in the layer below. To measure  $\mu_{eff}$ , we glued  $1 \text{ mm}$  glass beads in a monolayer to a glass slide. We then performed an inclined plane test with this system immersed in water, setting individual glass beads on top of the bead-covered slide and slowly tilting the slide until the loose beads started falling down. From this we obtained  $\mu_{eff} = 0.8 \pm 0.1$ . A force balance gives a prediction for the stress at the onset of granular shear to be  $\mu_{eff}\Delta\rho ga/15.3$ . This gravity-dominated prediction is plotted in Fig. 5. It is seen to match well with the measured onset stress  $\tau_{min}$  for particles between  $50$  and  $1125 \mu\text{m}$  in diameter. This suggests that the onset of shear thickening in the gravity-dominated regime is set by the shear stress required to initiate shear of the particles against gravity and friction.

Since the onset scaling for large particles is set by gravity, this suggests  $\tau_{min}$  can be lowered by density matching. We tested this by measuring steady state viscosity curves for  $100 \mu\text{m}$  polyethylene particles in silicone oil with a density different of about  $10^{-4} \text{ g/mL}$ . The mean value of  $\tau_{min}$  is shown in Fig. 5. While  $\Delta\rho$  was reduced by a factor of  $10^4$  compared to the non-density matched case, the onset stress was only reduced by an order of magnitude. In this case the density matched sample falls onto a similar scaling as was found for the glass for  $a \leq 25 \mu\text{m}$ . In many cases for particles even as large as  $100 \mu\text{m}$ , density matching can have no effect on the onset stress due to the significance of interparticle interactions. For cornstarch in water, density matching by adding CsCl to the water did not reduce the onset stress. For glass spheres in a heavy liquid  $\rho = 2.46 \text{ g/mL}$  (Cargille labs inorganic salt series) we found no measurable decrease in the onset stress compared to mineral oil or water, and found shear thinning below the onset as opposed to the Newtonian behavior found for glass suspensions whose onset is determined by the gravitational scaling [22, 23]. This suggests that in each of these cases, the stress scaling characterizing interparticle interactions which is dominant for smaller particles is already very close to the onset stress. This suggests that while density matching can lower the onset stress in the gravity-dominated regime, it cannot do so beyond the limits set by any other stress scales due to particle interactions. Thus we generally expect a larger effect of density matching for very large particles further into the gravity dominated regime.

In this set of experiments with a parallel plate setup, gravity caused particles to settle and initiating shear required exceeding the hydrostatic pressure of the top layer of particles only. In contrast, in a Couette cell with vertical walls a yield stress was found that scales with the hydrostatic pressure due to the full weight of the grains in the suspension pushing on the walls [45]. We now know that such a yield stress can hide shear thickening [23]. This suggests the yield stress from gravity is geometry dependent because of the directionality of gravity.

While this yield stress can hide shear thickening effects and move the onset [23], there is no indication that the shear thickening mechanism itself is geometry dependent. Thus a horizontal rheometer plate allowed the observation of shear thickening in suspensions of large particles without it being hidden by a yield stress.

## VI. SHEAR PROFILE

We next show shear profile measurements of both density matched and non-density matched suspensions to further study the role of gravity and the relevance of local constitutive relations beyond the onset of shear thickening.

To measure the shear profile we used a video camera with a bellows and magnifying lens to obtain a pixel size as small as  $20 \mu\text{m}$ . The camera was placed next to the standard parallel plate rheometer setup and focused on the outer edge of the sample in the plane of the shear direction and shear gradient. While there is some distortion from looking through the curved liquid-air interface, we can see individual particle motions to measure the shear profile at the edge of the sample. Videos were taken for constant shear rate measurements after the steady state was reached. Videos of the raw particle motions under shear are included in the supplementary material online. Local velocities are obtained by particle image velocimetry. Steady state shear profiles obtained by averaging the velocities at each height are. A small tilt of the camera causes a smoothing effect over about 4% in the depth.

We first describe results for a settling suspension of  $150 \mu\text{m}$   $\text{ZrO}_2$  spheres in mineral oil at  $\phi = 0.53$  with a gap  $890 \mu\text{m}$  wide. Velocity profiles are shown in Fig. 6 for a range of shear stresses, normalized by  $\tau_{max} \approx 10 \text{ Pa}$  to compare the form of the shear profile in different rheological regimes. Below  $\tau_{min} \approx 0.3 \text{ Pa}$ , we found no measurable particle motion up to a resolution of  $10^{-3}$  times the plate displacement. In this regime the particles remain settled due to gravity as expected based on the measurements of  $\tau_{min}$  in Sec. V. This also agrees well with the observations that the onset of shear thickening corresponds to the onset of dilation [1], since shearing of the grains is what results in dilation. Above the onset, we find a narrow shear band near the moving top plate. The width of the shear band increases as the stress is increased. Layering can clearly be observed at higher shear rates. Effects of this layering on the measured stress can be observed for suspension less than about few layers thick, where the layering can be frustrated at gap sizes corresponding to non-integer particle widths corresponding to higher stresses, but this contribution to the stress becomes negligible within measurement resolution above about 5 layers [24]. We performed similar measurements with glass particles in mineral oil with a gap size 12 particles wide as opposed to 6 particles wide with the  $\text{ZrO}_2$ . Results were qualitatively similar to the  $\text{ZrO}_2$  data, although layering

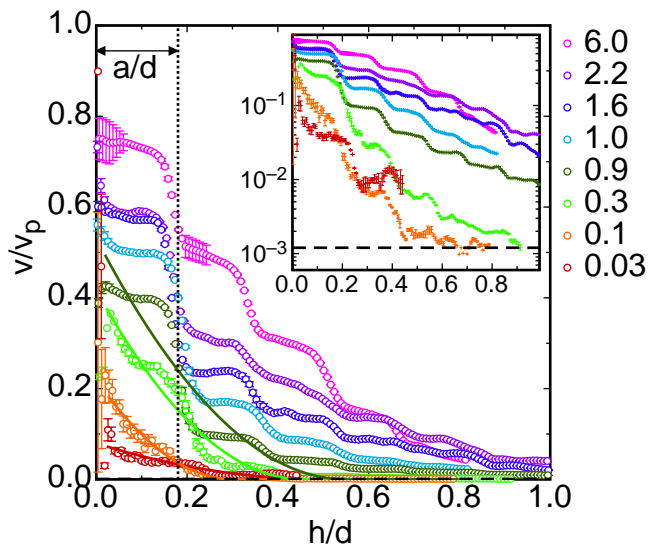


FIG. 6: Shear profiles at the plate edge in terms of normalized velocity vs. depth for settling particles of  $\text{ZrO}_2$  in mineral oil ( $\Delta\rho = 2.9 \text{ g/mL}$ ). Normalized shear stress  $\tau/\tau_{max}$  for each profile are shown in the key. Dashed line: upper bound of  $10^{-3}$  for a measurement at  $\tau < \tau_{min}$ . Dotted black line: depth equal to 1 particle diameter. Solid lines: fits of Eqn. 5 to the data for  $\tau < \tau_{max}$ . Inset: same data on log-linear scale. Videos are included in the supplementary material online.

was less prominent, appearing only clearly in the top two layers, as expected for a finite-size effect.

We next describe results for nearly density-matched  $135 \mu\text{m}$  polyethylene spheres in silicone oil at  $\phi = 0.55$  with a gap  $850 \mu\text{m}$  wide. The lighting used to take the videos heated the silicone oil by several degrees, so there is a slight density difference of about  $\Delta\rho = -0.01 \text{ g/mL}$  such that the particles are slightly buoyant, effectively reversing the direction of gravity. Because the smaller density difference moves the onset of shear thickening to very low shear rates, we did not obtain measurements of the shear profile below  $\tau_{min} \approx 0.01 \text{ Pa}$ . Velocity profiles are shown in Fig. 7 for a range of shear stresses, normalized by  $\tau_{max} \approx 0.5 \text{ Pa}$ . In the shear thickening regime, the velocity gradient in the bulk is so low that it appears nearly plug-like, with a shear band at the bottom plate and a layered structure at the top plate. The shear band now appears at the bottom plate and the direction of curvature of the shear profile is reversed due to the inversion of gravity. The shear band widened at higher stresses, similar to the case for the settling  $\text{ZrO}_2$ . Interestingly, for all three suspensions the layering was most pronounced near the top moving plate despite the gravity inversion.

These measurements also allow us to measure slip directly. When the particles were settled with the plate moving past, there was not even contact so the difference between plate and particle motions is not technically slip and should not be expected to follow slip correction models which usually assume a linear bulk velocity

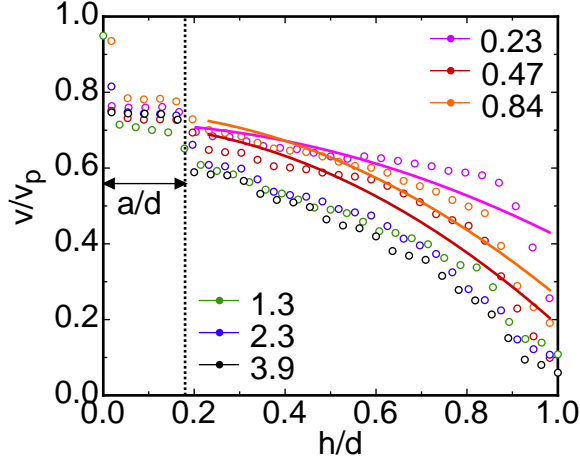


FIG. 7: Shear profiles at the plate edge in terms of normalized velocity vs. depth for nearly density matched polyethylene in silicone oil ( $\Delta\rho \approx -0.01$  g/mL). Normalized shear stress  $\tau/\tau_{max}$  for each profile are shown in the key. Dotted black line: depth equal to 1 particle diameter. Solid lines: fits of Eqn. 6 to the data for  $\tau < \tau_{max}$  with the substitution  $h/d \rightarrow 1 - h/d$  since the particles are lighter than the liquid. Videos are included in the supplementary material online.

profile. Settling and slip effects can be distinguished by comparing to the density matched case shown in Fig. 7 where the settling rate is much lower than the shear rate for all of the data shown. The difference between the speed of the top plate and neighboring particles in the more developed flow regimes is around 25%, roughly independent of shear stress. Since this does not change significantly at the boundary between shear thickening and shear thinning regimes, confirming that those rheological boundaries are not determined by slip. Since we are interested in mechanical response attributed to shear thickening, we do not consider it appropriate to ‘correct’ for slip. In any case, making a correction for slip does not significantly alter the shape of the viscosity curves nor move the regime boundaries in terms of stress because it only affects the shear rate. While it does slightly shift the magnitude of the viscosities reported, we do not make any conclusions based on the magnitude of the viscosity. The lack of contact between the particles and plate with settling is not problematic in terms of the mechanical response because viscous interactions within the liquid transmit stress between them just as well as hard contacts. This is confirmed by our observation that switching from smooth to rough plates does not change the stress scales or qualitative response.

### A. Local constitutive relations and the shear profile

Here we consider the significance of the shape of the shear profile in the shear thickening regime. Since the shear stress in a parallel plate geometry is independent of height, a local hydrodynamic constitutive relation  $\tau(\dot{\gamma}_l)$

dependent on a local shear rate  $\dot{\gamma}_l$  would correspond to a linear velocity profile. To allow for a non-linear steady state velocity profile, fixes have been introduced to make constitutive relations self-consistent by relating fluctuations in the local shear rate to an effective kinetic temperature [54] and by including the effect of the local variation in packing fraction on the viscosity [32, 54]. However, neither of these fixes determine the shape of the shear profile because they add additional free parameters so many velocity profiles are consistent with the constitutive laws, including the linear one. In granular shear flows, the initial inhomogeneity is usually attributed to dilation near the moving plate [42]. The question remains as to what determines the shape of the shear profile.

Here we propose that gravity and friction can account for the curvature in the shear profile. A non-linear shear profile could be the result of a constitutive relation that depends explicitly on height. Specifically, there can be frictional forces between particles due to the weight of the packing which increases with depth  $h$  into the sample relative to the top plate (for downward gravity) if the particles remain in contact via force chains. The simplest form for a local stress relation that includes gravity is

$$\tau = \eta_\nu \dot{\gamma}_l + \tau_g h/d + \tau_c \quad (3)$$

where  $\eta_\nu$  is the viscous hydrodynamic contribution to the viscosity, the gravitational stress scale  $\tau_g \equiv \mu\Delta\rho g d/15.3$  from Sec. V, and  $\tau_c$  represents any stresses that are independent of local shear rate and depth such as interparticle attractions. Rearranging gives the local shear rate

$$\dot{\gamma}_l = (\tau - \tau_c - \tau_g h/d)/\eta_\nu. \quad (4)$$

This implies a critical depth  $h_c/d = (\tau - \tau_c)/\tau_g$  at which the shear rate equals zero and beyond which there is no shearing of grains. This suggests the shear stress must exceed the sum of interparticle stresses ( $\tau_c$ ) and gravitational stress on the first layer of particles ( $\tau_g a/d$ ) to shear grains, the same condition for the onset of shear thickening shown in Fig. 5. The velocity profile can be obtained by integrating the local shear rate from Eqn. 4 over depth. There are two solution regimes: if  $h_c < d$ , then

$$\frac{v}{v_p} = \frac{\tau_g}{2\tau_\nu} \left( \frac{h_c - h}{d} \right)^2, \quad (5)$$

and if  $h_c > d$ , then

$$\frac{v}{v_p} = \frac{\tau - \tau_c - \tau_g}{\tau_\nu} \left( \frac{d - h}{d} \right) + \frac{\tau_g}{2\tau_\nu} \left( \frac{d - h}{d} \right)^2 \quad (6)$$

where the plate velocity  $v_p = d\dot{\gamma}$  and the viscous stress scale is defined by  $\tau_\nu \equiv \eta_\nu \dot{\gamma}$ . This suggests the curvature of the velocity profile is set by the ratio of gravitational

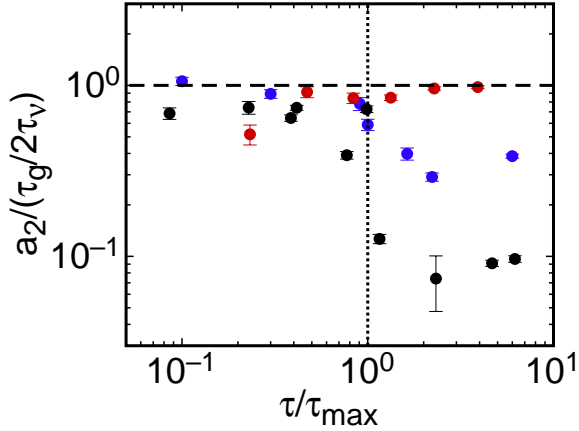


FIG. 8: Curvature  $a_2$  of velocity profiles normalized by the model prediction from Eqn. 6 with  $\tau_{min}$  is used as an estimate for the viscous stress  $\tau_\nu$ . The curvature  $a_2$  is obtained from the fitting the quadratic Eqn. 7 to data. Data is shown for different normalized shear stresses  $\tau/\tau_{max}$  for glass in mineral oil (black symbols,  $\Delta\rho = 1.58$  g/mL),  $\mu\text{m}$  polyethylene in silicone oil (red symbols,  $\Delta\rho = -0.01$  g/mL), and  $\mu\text{m}$   $\text{ZrO}_2$  in mineral oil (blue symbols,  $\Delta\rho = 2.9$  g/mL). The data collapse close to a value of 1 for  $\tau < \tau_{max}$  suggests the curvature of the shear profile is due to the weight of the particles on deeper layers which is transferred via frictional contacts in that regime.

to viscous stresses  $\tau_g/\tau_\nu$ . The velocity profile becomes linear in the limit where this ratio goes to zero ( $h_c > d$ ) as expected. These profiles are concave up, and become more linear with increasing  $\tau$  in qualitative agreement with the data in Fig. 6. These equations were written for the case where the effective gravity on the particles is downward. For the polyethylene data where the effective gravity is upward, then we have to make the substitution  $h/d \rightarrow 1 - h/d$  which reverses the concavity.

Because we are applying a continuum model to a system that is quantized due to layering, and the role of fluctuations in smoothing out mean shear profiles, we do not expect the gravitational model to be exact. Rather, the purpose is to test how relevant gravity is to the shear profile. To test this model, we fit the function

$$v/v_p = a_1 \frac{(h_c - h)}{d} + a_2 \left[ \frac{(h_c - h)}{d} \right]^2 \quad (7)$$

to the measured velocity profiles for each shear rate. Some of these fits are shown in Figs. 6 and 7. For  $\text{ZrO}_2$  and glass, it appears that  $h_c < d$  for  $\tau < \tau_{max}$  so we fix  $a_1 = 0$  according to Eqn. 5. The quadratic coefficient  $a_2$  can be compared to the prediction of Eqns. 5 and 6 with an estimate for the viscous stress  $\tau_\nu$ . At the onset of shear thickening the viscous stress must be enough to initiate shear so  $\tau_\nu \approx \tau_{min}$  as suggested by Sec. V. Since the shear rate increases slowly in the shear thickening regime for Discontinuous Shear Thickening, we will use

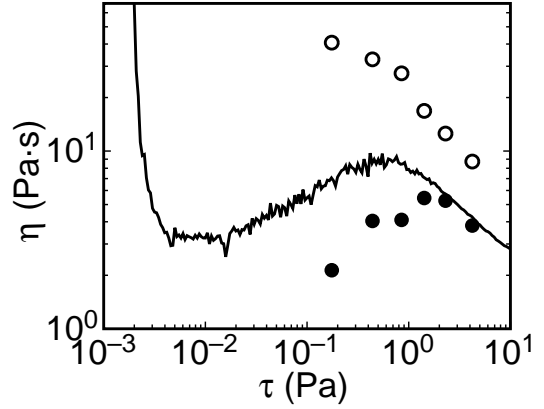


FIG. 9: Local viscosity curves for polyethylene spheres in silicone oil obtained from the shear profiles in Fig. 7. Open circles: local viscosity in bulk region. Solid circles: local viscosity in the shear band near the bottom plate. Solid line: global viscosity curve.

this estimate for the entire shear thickening regime. The measured curvature normalized by the predicted value  $a_2/(\tau_g/2\tau_{min})$  is plotted in Fig. 8 for each fit for  $\text{ZrO}_2$ , polyethylene, and glass. For  $\tau < \tau_{max}$ , the data for all three density differences collapse onto a single curve with  $a_2/(\tau_g/2\tau_{min}) \approx 1$ . This value is in agreement with the model which confirms the curvature of the shear profile is set by a balance of gravity-induced friction and viscous interactions. Because the data collapse works for systems of different sizes, it rules out the role of finite size effects in setting the velocity profile curvature.

For  $\tau > \tau_{max}$ , the different curvature values do not collapse onto a single curve, suggesting either that the model fails or at least that  $\tau_{min}$  is no longer a good approximation of  $\tau_\nu$  in this regime. Rather, the profiles appear to be closer to exponential (see inset of Fig. 6), similar to granular shear profiles of spherical particles [42]. This suggest that above  $\tau_{max}$  the shear profile could be that of a fully granular system where there is no need for a contribution of viscous hydrodynamics.

An alternate model attributes curvature in the shear profile to variations in the local packing fraction [32, 54]. In this model the small changes in packing fraction from dilation are significant because the viscosity divergence with packing fraction comes from the viscous lubrication layer goes to zero at the jamming transition. However, the curvature of the shear profile suggests stress is transmitted through frictional contacts so the strong packing fraction dependence of the viscous hydrodynamic part of the viscosity does not apply in this case, and the curvature cannot be attributed to packing fraction variation.

Local viscosity curves leads to a surprising result. The local viscosity can be calculated as the ratio of the measured global stress and the local shear rate from the derivative of the velocity profile. To qualitatively characterize the bulk region we use the mean slope of the velocity profile in the range  $0.2 < h/d < 0.8$ , and for the shear

band we use the mean slope in the range  $h/d > 0.85$  from the profiles in Fig. 7. The corresponding local viscosities are plotted in Fig. 9 along with the global viscosity curve. While the shear band shows shear thickening similar to the global curve, the bulk region appears to be everywhere shear thinning based on the local viscosity. The non-density matched data in Fig. 6 also corresponds to local shear thinning in the bulk, as the bulk is jammed corresponding to an infinite viscosity below  $\tau_{min}$ . Thus the region that qualitatively determines the global rheology is not the bulk but rather the near-wall region where the shearing occurs. This is not surprising from a granular or solid mechanics point of view where the global behavior is often determined by the failure in the weakest region.

Another test of the validity of local constitutive equations comes from comparisons of measurements in different measuring geometries. For a measurement in a cone and plate geometry the mean shear rate is independent of radius because the plate speed is proportional to the gap height at each point along a radius, while in a parallel plate setup the mean shear rate increases with radius because the plate speed is faster near the edge but the gap remains the same. Thus, assuming a local constitutive relation between shear stress and rate holds, an apparent viscosity curve measured in a parallel plate rheometer should be smoothed out compared to one measured in a cone and plate rheometer. However, a comparison of measurements of Discontinuous Shear Thickening in different geometries showed that the apparent viscosity curve from a parallel plate rheometer was *steeper* than that measured with a cone and plate rheometer [21]. This suggests that the mechanical stress response cannot be fully described by a local constitutive law between shear stress and rate.

To summarize this section, we can identify transitions in the shear profile with the stress scales that bound the shear thickening regime  $\tau_{min}$  and  $\tau_{max}$ . The onset of shear thickening corresponds to the onset of granular shear, and at lower shear stresses particles remain settled due to gravity or held together by other interparticle forces as described in Sec. V. In the shear thickening regime, the curvature of the shear profile suggests a balance between gravity-induced friction and viscous interactions can only hold if the weight of the packing builds up in deeper layers. This implies force chains between particles must extend from plate to plate. While the force chains are common to granular systems, the quadratic shear profile requires a balance between gravity-induced friction and viscous forces so is specific to suspensions. While we do see the shear profile change in different regimes, the remarkable feature of Discontinuous Shear Thickening is the large stress jump. The collapse of the curvature values in Fig. 8 for  $\tau < \tau_{max}$  suggests the viscous term  $\eta\nu\dot{\gamma}$  is nearly constant in the shear thickening regime, so the stress jump can not be attributed to viscous interactions. Instead, the stress jump must be hidden within the uniform stress term  $\tau_c$ , whose source we

will identify in Sec. VII. Thus the shear profile is only a measure of secondary stresses and not directly related to the mechanism for shear thickening. The fact that a local viscosity curve shows only shear thinning in the bulk suggests that local bulk constitutive relations relating shear stress and rate will not describe the mechanical response of Discontinuous Shear Thickening, but rather to understand the global mechanical response the boundaries must be considered.

## VII. NORMAL FORCES AND THE BOUNDARY CONDITION

In this section we use measurements of shear and normal stresses under different boundary conditions to show that the global mechanical response can be described by a frictional constitutive law rather than a viscous law.

### A. Frictional scaling

Here we compare steady state viscosity curves along with normal stress measurements for similar suspensions with different boundary conditions. The sample was 100  $\mu\text{m}$  diameter glass spheres in water at a packing fraction of  $\phi = 0.52$  ( $< \phi_c$ ). We first show results from a standard parallel plate setup (Fig. 1a) with a diameter of 50 mm which results in a better normal stress resolution than smaller plates. The shear stress  $\tau$  and normal stress  $\tau_N$  are shown in Fig. 10a as functions of shear rate  $\dot{\gamma}$  for a measurement in which the gap size is fixed at 0.72 mm. The region with slope greater than 1 defines the shear thickening regime. We find positive normal stresses, corresponding to the sample pushing against the plates, in agreement with other measurements of Discontinuous Shear Thickening [16, 21]. Not only is there a strong correlation between the shear and normal stresses, but they are on the same scale. The cutoff of  $\tau_N$  at the low end corresponds to the measurement dropping below the relative resolution of the normal stress of about 0.3 Pa.

We next use the walled rheometer setup without a liquid air interface as shown in Fig. 1b. In this case a sample of 500  $\mu\text{m}$  glass spheres in water was used; the larger particles were necessary to avoid them escaping through the gap between the side wall and top plate, but otherwise the samples behave in a qualitatively similar way in the normal parallel plate setup (see Fig. 5). The normal force on the top plate was fixed at 1 N (2040 Pa), consequently the gap size was allowed to vary. The viscosity curve is shown in Fig. 10a. In contrast to the standard parallel plate setup, the rheology is that of a yield stress fluid and there is no shear thickening regime. The qualitative difference of whether shear thickening or shear thinning was observed must be due to the difference in boundary conditions for the two experiments. Despite this, one common feature of both measurements is the connection of

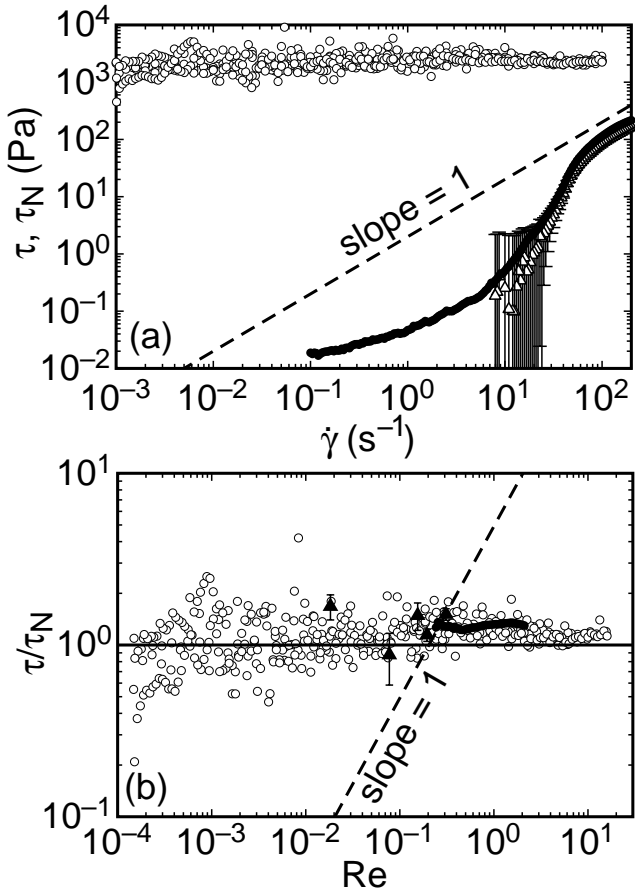


FIG. 10: (a) A comparison of flow curves measured with different boundary conditions for a sample of  $100\ \mu\text{m}$  glass spheres in water at  $\phi = 0.52$  ( $< \phi_c$ ). Solid circles: shear stress  $\tau$  from a fixed gap measurement with the standard parallel plate setup. Open triangles: normal stress  $\tau_N$  from the same measurement. The absolute uncertainty on the normal stress is 2 Pa, so the normal stress cannot be resolved at the low end. Open circles:  $\tau$  for fixed normal stress of 2040 Pa in the modified parallel plate setup with a hard wall. Dashed line: slope 1 corresponding to a Newtonian scaling for reference. (b) Circles: same data with the shear stress  $\tau$  normalized by normal stress  $\tau_N$  vs.  $Re = \rho d^2 \dot{\gamma} / \eta_m$ . Solid triangles: constant shear rate measurements in the standard parallel plate setup in which the normal force was recalibrated before each measurement. Solid line:  $\tau = \tau_N$  indicating a frictional scaling. Dashed line:  $\tau = \eta_m \dot{\gamma}$  corresponding to a viscous scaling.

the shear stress to the normal stress. We plot the ratio of stresses  $\tau/\tau_N$  vs. the Reynolds number  $Re_p = \rho d^2 \dot{\gamma} / \eta_m$  for both measurements in Fig. 10b. Additionally, we show steady state values for measurements taken at constant shear rate in the shear thickening regime in which the normal force was recalibrated relative to the static value before each measurement to optimize resolution of the relative normal force. The fact that these three data sets under different measurement conditions collapse onto the same curve shows that there is a global constitutive relation regardless of boundary conditions.

Since  $\tau/\tau_N$  is nearly constant over five decades of particle Reynolds number regardless of the boundary conditions suggests that the measured stresses are compressional in nature, such as frictional, rather than viscous in which case stresses should scale linearly with shear rate. This scaling can account for the constant stress term  $\tau_c$  in the constitutive relation of Eqn. 3, since it is independent of shear rate and height, but instead is dependent on the normal stress. A frictional scaling implies not only that stresses are redirected in different directions through the bulk of the suspension, a feature of granular materials in which forces are transmitted along chains of hard particles via frictional contact [37]. Additionally, it implies that positive pressures can be maintained on the system even without solid boundaries on all sides, the source of which will be investigated in Secs. VIII and IX.

### B. Transient normal force control measurements

We showed that for steady state measurements with very different boundary conditions the shear and normal stresses always had a fixed ratio near 1, thus the boundary condition determined whether or not shear thickening was observed. Here we show the universality of this result by showing that it applies even to transient measurements as the normal force boundary condition changes, and that shear thickening can be eliminated if the normal force is removed from the boundary as suggested by Ref. [21].

We performed normal force controlled experiments modeled after those of Ref. [21]. These measurements were done in the standard parallel plate setup in a normal force controlled mode. The normal force set point is zero relative to the rest state, with an initial gap of  $d = 1.08$  mm. The gap size is free to vary during the measurements to adjust the normal force back to the setpoint via a feedback loop. Initially the sample of cornstarch in water at  $\phi = 0.55 < \phi_c$  was at rest, then at time  $t = 0$  the shear rate was turned on and remained constant throughout the experiment. Examples of transient time series of the shear stress and normal stress are plotted in Fig. 11a for two different shear rates. For shear rates below the onset of shear thickening  $\dot{\gamma}_c \approx 11\ \text{s}^{-1}$ , the stress quickly came to near the steady state value within a fraction of a second and remained fairly steady there. For shear rates above  $\dot{\gamma}_c$ , the shear and normal stresses had a large peak initially, exceeding the steady state value by more than an order of magnitude. Even though the normal force set point was zero, the normal stress can be non-zero in the transient behavior as the gap adjusts via a feedback loop. Longer time series are shown in Fig. 11b along with the variation in gap size. Below  $\dot{\gamma}_c$  the normal force did not exceed the threshold to cause the gap to move. In contrast, above  $\dot{\gamma}_c$  the gap increased initially due to the transient normal force. The shear stress tracked the normal stress quite well throughout the entire transient process, and were similar in mag-

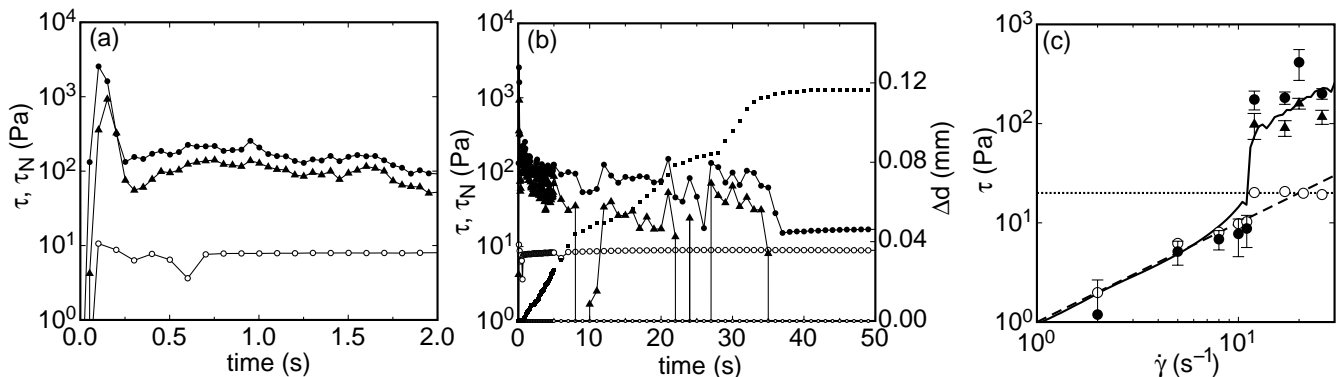


FIG. 11: (a) Transient time series of shear stress  $\tau$  (circles) and normal stress  $\tau_N$  (triangles) in normal force control measurements for cornstarch in water at  $\phi = 0.55 < \phi_c$ . The sample starts at rest then the shear is switched on at time  $t = 0$ . Circles: shear stress. Triangles: normal stress. Solid symbols: shear rate  $\dot{\gamma} = 26 \text{ s}^{-1}$  (above  $\dot{\gamma}_c$ ). Open symbols:  $\dot{\gamma} = 8 \text{ s}^{-1}$  (below  $\dot{\gamma}_c$ ). (b) Same data as panel a, but extended to longer times to see the steady state behavior. Right axis: change in gap size  $\Delta d$  (small squares). (c) Effective viscosity curves obtained from transient measurements. Solid circles: transient shear stress averaged between 0.4 and 1.0 s after shear starts. Solid triangles: transient normal stress averaged over the same time. Open circles: steady state shear stress at the end of the time series where  $\tau_N$  was below the resolution limit for each shear rate. The shear stress is limited to the normal stress resolution in this case so shear thickening is suppressed. Solid line: stress as a function of shear rate obtained from a steady state viscosity curve for the same sample with fixed gap size. Dashed line: Newtonian scaling.

nitude. The stresses each decreased as the gap increased, and the gap stopped increasing when the normal stress dropped below the feedback threshold. Beyond this point the stresses and gap size remained constant, which was measured for at least 200 s in each experiment to confirm that the system was in a steady state.

We summarize the normal force control experiments with effective viscosity curves in Fig. 11c. We show the transient shear and normal stresses averaged between 0.4 and 1 s after the shear was started as solid circles. Because the response time of these samples to dramatic changes is typically a fraction of a second, while the normal force control feedback loop has a longer timescale, these transient results effectively have a fixed gap boundary condition and show the same qualitative shear thickening as steady state behavior for fixed gap measurements. For reference, the solid line indicates a steady state viscosity curve with fixed gap size. Differences between the solid circles and solid line beyond the measurement resolution indicate a difference between steady state and transient measurements. Stress values taken from the end of the test where  $\tau_N = 0$  ( $\pm 20 \text{ Pa}$ ) and the system was in a steady state are shown as open circles in Fig. 11c. The effective viscosity curve based on this data is consistent with a Newtonian scaling at shear rates below  $\dot{\gamma}_c$ . Above  $\dot{\gamma}_c$ , the shear stress values match up with the normal stress feedback threshold. This can be understood since a normal stress of that magnitude is not enough to trigger the normal force control feedback loop but can still couple to the shear stress. The strong shear thickening in the fixed gap data and transient data is totally absent from the  $\tau_N = 0$  data. We note that there is no significant dependence of viscosity curves on gap size in this range [24], so the difference must be due

to the fact that the normal force is fixed to be zero. This shows that a positive normal stress of comparable magnitude is required to achieve the shear stress associated with shear thickening, and in the absence of this confining stress, shear thickening cannot occur, as was suggested by Ref. [21]. Without making any assumption about the mechanism for coupling between the normal and shear stresses at values below the normal stress feedback threshold, the open circles in Fig. 11c put an upper bound on the viscous and other non-compressive contributions to suspension viscosity and show that they are not responsible for Discontinuous Shear Thickening.[78]

We have noted that the normal and shear stresses track each other quite well in normal force control measurements. In fact, in all of the various types of experiments on dense suspensions tried where normal stresses and shear stresses were compared they tend to track each other quite well. For example, we attempted measurements with a fixed normal stress  $\tau_N = 0$  and fixed shear stress greater than the normal stress feedback threshold. Since the shear stress is the dominant control parameter of the rheometer, the shear stress reached the set value but the measurements never reached a steady state because the normal stress could not drop, causing the gap to increase until the top plate detached from the sample. In another set of experiments where stress fluctuations were measured in the steady state [16], fluctuations of the normal stress and shear stress were found to be strongly correlated. This helps explain an earlier result in which an apparent viscosity curve no longer showed shear thickening when positive fluctuations in the shear stress in the steady state were removed from the data [15]. Since the shear stress fluctuations were associated with the normal stress, that was in essence showing an

effective viscosity curve with no normal stress. Another example was shown in measurements of finite-size effects very small gap sizes[24], in which the normal stress scaled with and was close in magnitude to the shear stress as it varied with gap size.

## VIII. VISIBLE BOUNDARY CONDITION

The previous section showed that the boundary condition is an important factor in shear thickening. In this section we show surface images to identify the boundary conditions so we can formulate a model for the measured stresses in Sec. IX.

### A. Boundary at rest

We first show images of the surface of suspensions at rest for comparison. The samples consisted of 135  $\mu\text{m}$  polyethylene spheres density matched in silicone oil, which are opaque and do not settle. These suspensions were placed in a  $H = 1.3$  mm deep layer and viewed from the top with direct lighting as shown in Fig. 12. The series was taken by starting at a high packing fraction well above the jamming transition, then adding oil to reduce the packing fraction for each successive image. At each packing fraction the sample was vibrated at 40kHz with a sonicator for 1 min, tilted during and after sonication to observe whether or not shear occurred, then allowed to rest before the image was taken.

For the highest packing fractions  $\phi > 0.64$ , the suspension surfaces appear dry and rough and did not flow under tilt during or after sonication. For  $0.64 \geq \phi > 0.57$  they appear wetter but still rough. In this range the samples did flow while being sonicated, they did not flow at infinitesimal tilt angles (measured at  $\sim 1^\circ$ ). However, for several of the packing fractions in this range there was a critical tilt angle  $\Theta$  above which flow could be found. For  $\phi \leq 0.57$ , the samples appear very shiny and smooth, and they flowed even at infinitesimal tilt angles.

We can connect the value of the critical tilt angle  $\Theta$  for flow to the yield stress of the suspension. For a tilt angle  $\Theta$ , the stress applied by gravity parallel to the surface is  $\rho g H \sin \Theta$  which is shown in Fig. 13 for packing fractions in which one was measured. We compare this to the yield stress  $\tau_y$  obtained from rheometer measurements as the limiting stress in the zero shear rate limit. For  $\phi < 0.58$ , we measured no yield stress, within a resolution of  $10^{-3}$  Pa. There is a relative uncertainty of about 0.005 in the packing fraction measurements for the yield stress due to the process of loading the sample. Within this uncertainty, the shear stress provided by gravity at the onset of shear under tilt matched with the measured yield stress in the rheometer. This confirms that the visible changes in the surface correspond to changes in the yield stress.

Similarly, the roughness of the surface of a suspension can be used as an indicator of the yield stress. At each packing fraction shown in Fig. 12 for  $\phi > 0.57$ , the sample surface has roughness on a macroscopic scale, i.e. much larger than individual particles. If an asperity of height  $H$  forms on the upper surface of a fluid it can remain stable if the yield stress exceeds a value on the scale of  $\rho g H$ . Thus the maximum asperity size seen on the surface of a suspension can be used as a rough indicator of the magnitude of the yield stress of a suspension. For these samples we observed asperities on the order of 1 mm at the highest packing fractions, consistent with the measured yield stresses on the order of 10 Pa and the value  $H$  used in the gravitational stress scale.

At the particle level, slightly different effects become visible at the surface. If a suspension is unjammed there is free space for the particles to rearrange, so any particles on the surface will be pushed by surface tension to the interior (assuming the liquid wets the particles, which is also a requirement to observe shear thickening [23]), resulting in a flat and shiny surface. In a jammed system, hard particle contacts or other forces counter the force of surface tension, so particles remain on the surface remains rough on the particle scale. If the particles are between about 0.1 and 100  $\mu\text{m}$ , then the grains are large enough to diffuse light and small enough that they cannot be seen individually, so the surface appears rough by eye. Thus a simple indicator of whether or not a suspension is jammed is whether the surface appears rough or smooth. This easily visible indicator of jamming contrasts with the case of dry grains, where there is no such indicator. The interstitial liquid allows this sensitive measurement by eye because changes in the fluid level at the surface due to changes in packing density only have to be on the scale of a particle size to dramatically change the surface appearance.

The critical packing fractions for the transitions in Fig. 12 match up with those usually found for the jamming transition [38]. The transition at  $\phi = 0.64$  corresponds to random close packing for frictionless spheres, above which packings are jammed and below which they can flow [65]. When comparing to other published values for critical packing fractions, It is reasonable to expect an absolute uncertainty in the range of 0.01 in the packing fraction due to factors such as a finite size effect and polydispersity in the particle sizes, and sample preparation. Experimentally it is usually found that packings of spheres remain mechanically stable, i.e. have a yield stress down to packing fractions around 0.56-0.60 depending on density difference  $\Delta\rho$ , called random loose packing [44, 66]. Packing fractions closer to  $\phi = 0.64$  can only be reached if the packings are vibrated which mobilizes the particle contacts, effectively eliminating the effect of friction [58]. This explains why in the range  $0.64 \geq \phi > 0.57$  our suspensions flow under sonication but are otherwise jammed.

We note the visible transition at  $\phi = 0.64$  in Fig. 12 is not always clearly observed, depending on sample prepara-

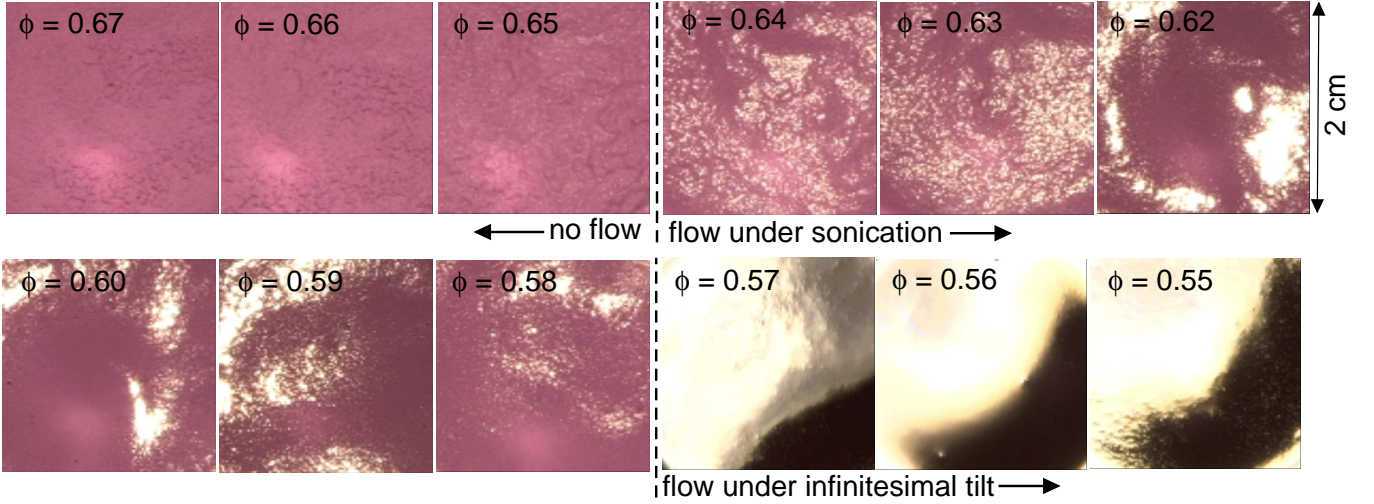


FIG. 12: Top views of a static layer of  $125 \mu\text{m}$  polyethylene spheres density matched in silicone oil. The layer was  $1.3 \text{ mm}$  deep and each image is  $2 \text{ cm}$  on a side. Images were taken for different packing fractions given in the corner of each panel. Lighting was direct to emphasize changes in reflectivity. Packing fractions  $\phi > 0.64$  did not flow under any amount of tilt. Packing fractions  $0.64 \geq \phi > 0.58$  flow while being sonicated, but after stopping sonication, these suspensions no longer flowed at small tilt angles. Packing fractions  $\phi \leq 0.57$  flow under even small tilt ( $\sim 1$  degree). The reflectance of the surface was so high for  $\phi \leq 0.57$  that the camera became oversaturated by the direct reflection of the light.

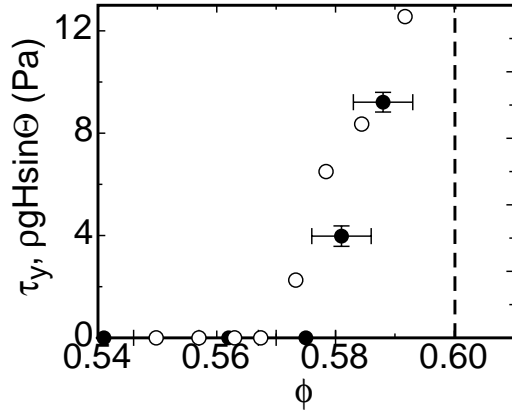


FIG. 13: Open symbols: gravitational stress  $\rho g H \sin \Theta$  required to initiate shear under tilt for the suspensions shown in Fig. 12. The minimum tilt angle  $\Theta$  required for shear is measured relative to a horizontal surface. Dashed line: threshold packing fraction above which the sample did not flow at any tilt angle (without sonication). Solid symbols: yield stress  $\tau_y$  obtained from viscosity curves in the rheometer. The jamming transition at  $\phi = 0.57$  above which there is a yield stress coincides with the visible change in the surface shown in Fig. 12.

ration. If we do not sonicate but instead mix with a spatula, the samples can appear to be dry until they are diluted all the way down to  $\phi = 0.57$ . This could be because without the mobilization of particle contacts allowed by sonication, the suspension may not be able to pack in space above  $\phi = 0.57$ , so to make up the extra space the liquid must retreat into the interior. Despite

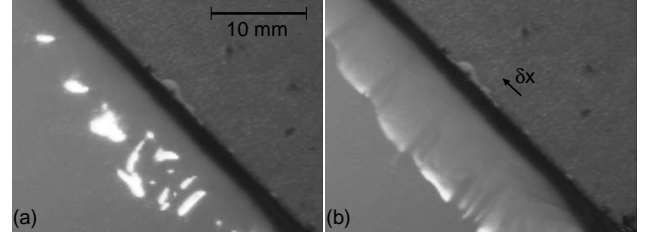


FIG. 14: Top views of a  $2.4 \text{ mm}$  deep layer of cornstarch in water. (a): Below  $\phi_c$  in a shear cell at rest. (a) at a shear rate above  $\dot{\gamma}_c$ , taken after a shear displacement of  $\delta x = 6.4 \text{ mm}$  relative to panel a. Dilation can be observed as an increase in surface roughness near the wall. See supplementary material online for a full video. **Retake images with particle tracers to better show strain and that shear occurs in the dilated region. Change lighting to get rid of black band.**

this hysteresis effect in the visible transition at  $\phi = 0.64$  during preparation, rheology measurements with pre-shear consistently show the onset of a yield stress at the same packing fraction.

## B. Dilation

We just demonstrated that a visible change in the surface of a suspension can correspond to a qualitative change in the mechanical rheology. A similar correspondence has been noted among the papers that have made connections between dilation and Discontinuous Shear Thickening, several found a visible change in the surface

of suspensions at the onset of shear thickening [1, 10, 57]. It was understood early on that this was due to dilation [1]. When grains dilate under shear, they take up more space than at rest, and consequently the liquid is then sucked away from the boundary into the enlarged gaps between grains, so the surface appears rough by eye.

This visible effect of dilation is shown for a suspension of cornstarch ( $14\ \mu\text{m}$ ) in water below  $\phi_c$  in Fig. 14. The suspension was in a 2.4 mm deep layer and viewed from above. One of the side walls could be displaced to shear the suspension. Before shear the surface of the suspension looked wet and shiny, as seen in panel a. When the upper right wall was sheared at a rate exceeding the onset of shear thickening the nearby suspension appeared rough, shown in panel b. As soon as the shear rate dropped below the onset of shear thickening, the surface appeared smooth and shiny again. A movie is included as supplementary material online.

Usually we find suspensions will show Discontinuous Shear Thickening in rheological measurements if the surface changes from shiny to rough when sheared, indicating dilation. At low packing fractions, the surface remains smooth under shear because the packing fraction is too low for granular dilation to affect the surface, since volume changes from dilation are typically only a few percent [43, 44]. Alternatively, if the suspension has a yield stress, the surface may be always rough and not change with shear rate, even if the packing still dilates with shear. Thus, the conditions where a change in the surface from dilation is observed seem to correspond to the conditions for suspensions to show Discontinuous Shear Thickening.

There is a notable exception to the rule that a visible change in the surface from dilation indicates shear thickening. Settling particles in a Couette cell were seen to dilate but did not shear thicken, instead a yield stress was measured [1, 45]. The weight of the particles in a vertical column of height  $H$  pushes on the side walls which are supposed to shear, resulting in a yield stress on the scale of  $\Delta\rho gH$  which can be on the order of kPa [45], well above the shear thickening stress regime which we observed for glass spheres from 10-100  $\mu\text{m}$  in a parallel plate geometry which does not have this yield stress (see Fig. 18). In the case of vertical walls, the side of the suspension is still jammed at rest which prevents shear thickening, but the top is not, so the suspension falsely appears unjammed when viewed from the top. In such cases, the dilated and unjammed regions are local, so the earlier claim that visible dilation implies shear thickening does not necessarily apply if the suspension is so inhomogeneous that jamming is localized. A more general conclusion is that dilation is necessary for Discontinuous Shear Thickening but not sufficient because shear thinning stresses must be small compared to shear thickening stresses or else the shear thickening will be hidden [23].

Now that we have established the importance of the boundary condition, we want to directly view what is changing at the boundary on the microscopic scale. We

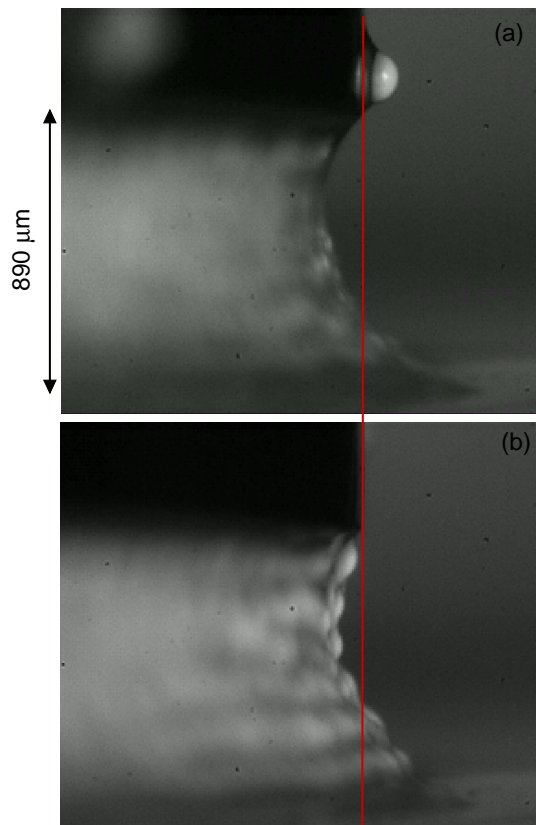


FIG. 15: A view of a suspension of  $150\ \mu\text{m}$   $\text{ZrO}_2$  particles in mineral oil in the standard parallel plate setup with a gap of  $890\ \mu\text{m}$ . The view is at the side of the sample, focused tangent to the surface to view radial variations in the boundary position. The rest of the image is out of focus because of the large amount of depth in the image. (a) The suspension at rest. (b) The suspension is sheared at constant shear rate of 3 Hz corresponding to  $\tau_{max}$ . It can be seen that shear results in both dilation of the suspension and increased local curvature at the surface. Red lines: reference line indicating the plate edge. See supplementary material online for a full video.

use a sample of  $150\ \mu\text{m}$  diameter  $\text{ZrO}_2$  particles in mineral oil at  $\phi = 0.54$  in a standard parallel plate rheometer setup with a gap size of  $890\ \mu\text{m}$ . These particles were chosen because they are opaque and large enough to be easily viewed individually. A video camera was pointed at the side of the sample, focused tangent to the surface to best view any radial variations in the boundary position due to dilation. The sample is shown at rest in Fig. 15a, in which case it had a smooth surface. The sample is shown in panel b at a steady shear rate of  $3\ \text{s}^{-1}$ , corresponding to  $\tau_{max}$  at the upper end of the shear thickening regime. A movie is included in the supplementary material online. The boundary appears bumpy as particles penetrate the liquid-air interface. The penetration of the liquid-air interface by the particles can also be seen in the shear profile videos of polyethylene included in the supplementary material. By reference to the edge of the rheometer plate (red line), it can be seen that the

sample has expanded radially relative to the rest state by about  $50 \mu\text{m}$ , corresponding to  $0.3a$  or a volume increase of 0.8%.

## IX. CAPILLARY FORCES

In the previous section showed that when a dense suspension dilates under shear, the particles penetrate the liquid-air interface. The curvature of the liquid-air interface caused by this can produce stresses from surface tension. It has been suggested that capillary forces at boundaries could play an important role in suspension rheology [59–61]. To understand the consequences of surface tension at the boundary we work through a proposed mechanism leading to an increased shear stress. When particles to poke out the edge of the suspension to create a curved liquid-air interface, the scale of the radius of curvature  $r$  of the liquid-air interface is set by the particle size  $a$ . This produces a stress from surface tension pushing the particles towards the interior of the suspension on the scale of  $\gamma/r$ , or  $\gamma/a$ , which can be on the order of 100 Pa for  $100 \mu\text{m}$  particles, a significant stress in terms of the rheological measurements. If the particles were not tightly packed, they would be pushed to the interior of the sample by this stress. However, the fact that the particles continue to penetrate the surface in the steady state implies that there are force chains that can transmit the stress through the packing, which can be static in the jammed case but may be dynamically changing in the case of dilation under shear. The stress from surface tension can then be considered a confining stress on the packing which is transmitted throughout the suspension by these force chains. In a granular packing, forces tend to be redirected easily as contacts between particles can occur at a variety of angles, so a confining stress on one side will lead to a similar normal stress being felt on the top and bottom plates. These normal stresses between particles result in shear stresses by frictional contacts with the rheometer plates, as was seen in Figs. 10 and 11. In the remainder of this section we quantitatively connect the measured shear stresses to the stress scale from surface tension  $\gamma/a$  to test this model.

### A. Relating dilation to confining stress

To quantify the dilation, we measured the mean radial displacement of the surface during shear seen in a tangent view as in Fig. 15. We do this for several different steady state shear rates in a sample of opaque  $135 \mu\text{m}$  polyethylene in silicone oil at  $\phi = 0.56$ . For each measurement, we started the sample at rest, then sheared at a constant shear rate until the stress reached a steady state, then stopped the shear to observe the relaxation to rest, then repeating the cycle of shear followed by resting a total of 5 times. The edge of the sample was tracked throughout these measurements. The dilation  $\delta$  was measured

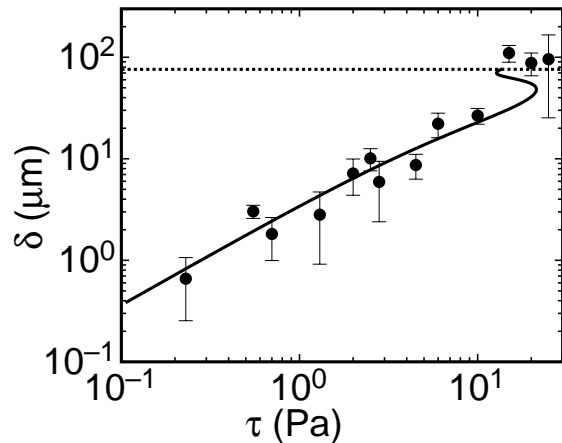


FIG. 16: The radial dilation  $\delta$  measured as a function of shear stress for  $135 \mu\text{m}$  polyethylene in silicone oil. Solid line: relationship between  $\delta$  and  $\tau$  for a model in which there is a confining stress from surface tension  $\tau \propto \gamma/r(\delta)$  where the local radius of curvature  $r(\delta)$  is determined geometrically. A proportionality coefficient of 0.14 shifting the curve horizontally is used to fit the data. Dashed line: dilation value where the contact line is expected to reach the 2nd layer of particles resulting in a dramatic increase in confining stress with dilation.

as the mean radial displacement of the edge between the steady state shear and rest states, averaging over the height of the sample and over at a period of at least 10 s and at least a strain of 2 in the steady state for each experiment. The measured dilation is plotted versus the corresponding steady state stress values in Fig. 16. Plotted error bars correspond to the standard deviation of  $\delta$  measured over the 5 cycles. All points shown correspond to the shear thickening regime and higher stresses. At lower stresses we could not resolve any dilation with a resolution limit of  $0.5 \mu\text{m}$ . The upper end of the shear thickening regime corresponds to  $\tau_{max} = 2 \text{ Pa}$  for this sample.

We can calculate a typical radius of curvature of the liquid-air interface as it contracts for a given particle dilation  $\delta$  given the contact angle and conservation of volume. This allows us to estimate a confining stress scale from surface tension  $\gamma/r(\delta)$ . Details of this calculation are shown in the appendix. Briefly, the initial state with a relatively large radius of curvature corresponds to  $\delta = 0$ . As  $\delta$  increases, the surface becomes more curved and the radius of curvature decreases, with the scale of the radius of curvature set by the interstitial gap size when the dilation is around a particle radius. This model prediction is plotted in Fig. 16 where  $\delta$  is plotted vs. the predicted stress scale  $\gamma/r(\delta)$ . A free parameter for the scale factor of 0.14 on the stress scale is used to fit the data. The qualitative agreement in the model slope with the data in Fig. 16 confirms that the confining stress scaling as  $\gamma/r$  is a good estimate for the measured shear stress. The fit coefficient on the order of 1

confirms that the amount of dilation is on the right scale to provide the measured stress. Fig. 16 shows a single scaling for the dilation with stress through the transition from shear thickening to shear thinning at  $\tau_{max} = 2$  Pa, supporting a direct relation between dilation and shear stress. Since the stress/shear-rate curve corresponds to Discontinuous Shear thickening, this implies the dilation  $\delta$  increases rapidly with shear rate in the shear thickening regime, then increases less rapidly above  $\tau_{max}$ .

The dotted line in Fig. 16 corresponds to the dilation value where the contact line is expected to reach the 2nd layer of particles from the surface (see appendix for calculation), at which point the confining stress should increase rapidly as more contacts are made with small curvature. Because the calculation of confining stress from dilation is not monotonic around this region, the dilation is not single-valued function of confining stress. The lower portion of the curve is expected to be unstable since more dilation would provide less of the confining stress required to confine the suspension to a smaller volume. The agreement of the dilation measurements with the dotted line beyond the point where the calculation becomes multi-valued supports this interpretation.

As the dilation increases further into the interior, a lower limit for the value for the curvature must be reached as it is limited by the interstitial gap size. The corresponding limiting confining pressure has been measured in an analogous system in which a fluid interface was driven through a porous medium, in which case the required driving pressure went to  $0.7\gamma/a$  in the limit of zero flow rate [62]. This confining stress sets the scale for the upper bound on the component of the shear stress due to capillary forces on the order of  $\gamma/a$  in the limit of large  $\delta$ . The value of  $\tau_{max} = 2$  Pa corresponding to the data in Fig. 16 is significantly below the limiting confining stress regime, suggesting that the dilation by a fraction of a particle width was enough to obtain a fully developed shear flow and the limiting confining stress is not necessarily reached in the shear thickening regime.

## B. Surface tension scaling

To further understand the role of capillary forces, we performed a set of rheological measurements in which we varied the surface tension of the liquid-air interface. To vary this surface tension, we added surfactant to 100  $\mu\text{m}$  glass spheres in water. The surfactant used was Palmolive dish detergent and first mixed in water above the critical micelle concentration which reduces the surface tension with air by about a factor of 3 compared to pure water and air. Viscosity curves are shown with and without surfactant and at different packing fractions are shown in Fig. 17. We first compare the viscosity curves for jammed suspensions at  $\phi = 0.59 > \phi_c$ . These viscosity curves correspond to yield stress fluids. The value of the yield stress is reduced by a factor of 2.4 with the addition of the surfactant, about the same as the surface

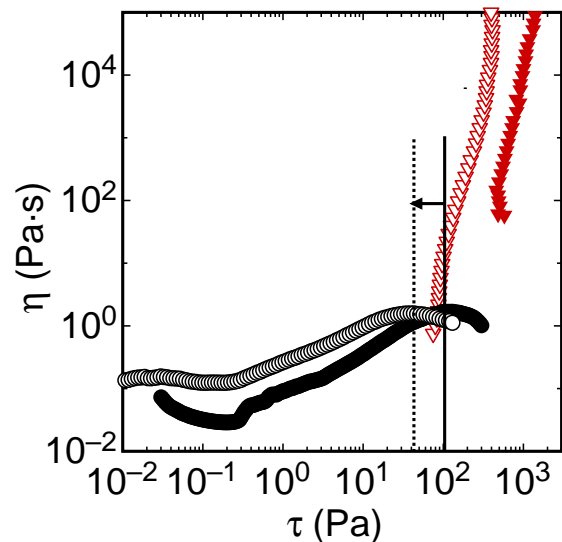


FIG. 17: Viscosity curves for 100  $\mu\text{m}$  glass spheres in liquids with different values of surface tension. Solid symbols: particles were suspended in water. Open symbols: particles were suspended in water with surfactant (above the critical micelle concentration). Triangles (red online):  $\phi = 0.58 > \phi_c$ . Circles:  $\phi = 0.56 < \phi_c$ . Solid line:  $\tau_{max}$  without surfactant. Dotted line:  $\tau_{max}$  with surfactant. Both  $\tau_{max}$  and  $\tau_j$  decreased when the surface tension was reduced.

tension was reduced.

We next compare the viscosity curves at  $\phi = 0.56 < \phi_c$  in Fig. 17. The vertical shift in the viscosity at low shear rates can be attributed to the increase in the zero shear viscosity with the addition of the surfactant. In terms of stress scales, there is a decrease in  $\tau_{max}$  by a factor of 2.4 when the surfactant is added, and no resolvable change in  $\tau_{min}$ . The reduction in both  $\tau_{max}$  and the yield stress  $\tau_j$  is comparable to the reduction in surface tension with the addition of surfactant, again consistent with a model in which these stresses scale with surface tension.

We note that in principle the addition of surfactant can change other relevant parameters. The stress from surface tension on a boundary typically scales as  $(\gamma/r) \cos \theta$  where  $r$  is the radius of curvature and  $\theta$  is the contact angle, where both  $\gamma$  and  $\theta$  can vary with the addition of surfactant. The addition of a surfactant can reduce  $\theta$  could increase in the stress from surface tension. However, we start with a liquid that wets glass pretty well, as this is a requirement to observe shear thickening [23], so  $\cos \theta \approx 1$  even before the addition of surfactant. The addition of surfactant can also affect the value of  $\tau_{min}$  in cases where the particle-liquid surface tension is dominant [23], but for these 100  $\mu\text{m}$  glass spheres in a wetting liquid the dominant force affecting the onset is gravity (Fig. 5).

The results in Fig. 17 suggested that the upper stress scales  $\tau_{max}$  and  $\tau_j$  scale with the surface tension at the liquid-air interface. The corresponding confining stress from surface tension when particles set the radius of cur-

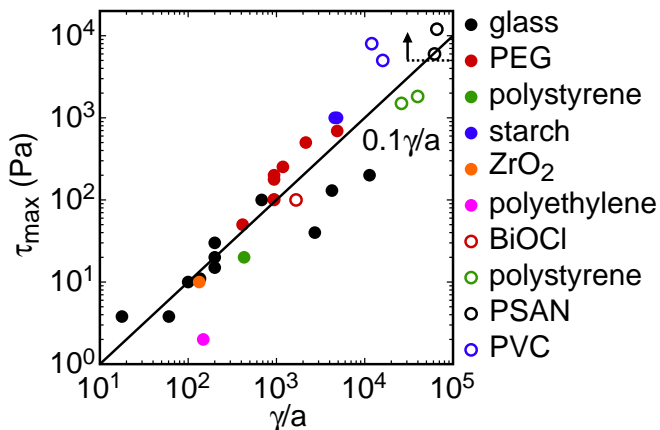


FIG. 18: The stress at the upper boundary of the shear thickening regime  $\tau_{max}$  for a variety of suspensions plotted against the confining stress scale from surface tension  $\gamma/a$ . Particle materials are listed in the key. Solid symbols: measured by us. Open symbols: measured by other groups: red [14], green [63], **include data from Ref. [6]**, black and blue [2]. The solid line corresponds to a scaling  $\tau_{max} \propto \gamma/a$ . Dotted line: lower bound on  $\tau_{max}$  for measurements in which  $\tau_{max}$  was not reached [11], which often occurs in colloid measurements.

vature at the surface is  $\gamma/a$ . To more generally test this relationship including the size scaling, we plot measured values of  $\tau_{max}$  vs.  $\gamma/a$  for the wide range of Discontinuous Shear Thickening suspensions we have studied in Fig. 18. Each point corresponds to a different suspension, with a wide range of different particle materials, shapes and sizes, and different liquids. We have also included data from other papers in cases where  $\tau_{max}$  was measured. A line scaling as  $\gamma/a$  is also plotted for reference. It is seen that for this wide variety of suspensions,  $\tau_{max}$  falls in a band that scales as  $\gamma/a$ . We note that for each Discontinuous Shear Thickening suspension we have studied, the two stress scales  $\tau_{max}$  and  $\tau_j$  are always within an order-of-magnitude of each other, as was seen for example in Fig. 17 and Ref. [22], suggesting that  $\tau_j$  also scales with  $\gamma/a$ . In many measurements of colloids, an upper bound on the shear thickening regime was not reached. If there is an upper bound, it would have to be above the range measured. This is especially a problem with colloids because the expected scale of  $\tau_{max}$  for small particles exceeds the measuring range of most rheometers. This lower bound on  $\tau_{max}$  based on the limited measuring range is illustrated as the dotted line in Fig. 17, using data from Ref. [11] as an example.

There is variation in the value of  $\tau_{max}$  in the band shown in Fig. 18 by about an order of magnitude. There are many factors that could contribute to the precise value of the confining stress and the resulting shear stress. For example, the normal stresses do not have to be exactly the same on each surface as would be the case for a pressure acting on a fluid. Instead the stresses are related by a coefficient of order 1 [64]. Since the confining

stress can put a normal stress on the top plate via chains of hard particle contacts, then a component of the shear stress comes from friction, related to the normal stress by a coefficient of friction as seen in Fig. 10. The contact angle  $\theta$  has been left out of the force equation since it is not known or easily measured in many cases. What exactly sets the mean radius of curvature of the liquid-air interface at  $\tau_{max}$  is not yet clear but it is probably determined by dilation which is still not well-characterized in dense suspensions. Geometric factors including particle shape and roughness also should play a role that has not yet been studied. Considering all of these dimensionless factors of order 1 that can affect the shear stress which we do not have values for, the stress scale of  $\gamma/a$  will remain an order of magnitude scaling estimate for  $\tau_{max}$ .

We now address why surface tension determines  $\tau_{max}$  and  $\tau_j$  rather than  $\tau_{min}$ . We already argued that the confining stress from surface tension produces normal stresses between particles and the walls that results in a shear stress via friction. This confining stress increases precipitously in the shear thickening regime as the amount of dilation increases with shear rate. The maximum confining stress from surface tension should be on the order of  $\gamma/a$ . Beyond that point, any additional shear stress must come from other sources, which are likely weak compared to the confining stress if shear thickening is observed, so the viscosity should drop off beyond the maximum confining stress. Thus the maximum confining stress should correspond to  $\tau_{max}$ . Above  $\phi_c$  where the suspension is jammed, particles penetrate the surface even without shear, so the yield stress scale  $\tau_j$  should be set by the confining stress.

## X. SOLID BOUNDARIES

In the previous section we showed that under boundary conditions such that particles penetrate the liquid-air interface, surface tension provides a confining stress which sets the scale of the stress response, specifically  $\tau_{max}$  and  $\tau_j$ . While a liquid-air interface at the boundary is typical for rheometer measurements, closed systems with solid walls are also of interest. In this section we will generalize the role of the confining stress from different sources to understand the rheology of dense suspensions in closed systems.

For measurements in a closed system, we used the parallel plate setup with solid walls shown in Fig. 1b. The hard walls confined large grains within the container volume without the need for the surface tension of the liquid, so we can determine the role of the liquid by comparing measurements with and without liquid. We first show stress/shear-rate curves for shear rate controlled measurements of dry 500  $\mu\text{m}$  glass spheres in Fig. 19. Without liquid, the packing fraction is determined by the container volume which can be varied with the gap size. Thus, for a series of measurements with a fixed volume of particles, the gap height determines the packing frac-

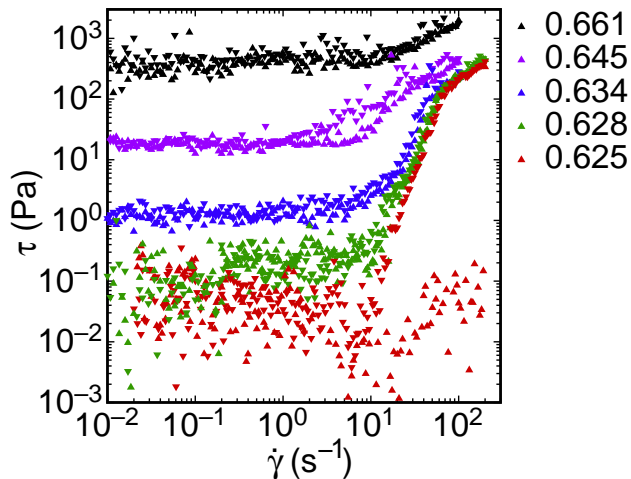


FIG. 19: Stress vs. shear rate curves for 500  $\mu\text{m}$  diameter glass spheres in a solid-walled rheometer with *no liquid*. Colors correspond to different packing fractions shown in the key. Discontinuous Shear Thickening is still seen, confirming that hydrodynamic interactions are not necessary for shear thickening.

tion, with smaller gaps corresponding to higher packing fractions. We give relative packing fraction values accurate to 3 decimal places to compare curves in Fig. 19, but absolute uncertainties on packing fractions are still around 0.01.

An important result from Fig. 19 is that the curves show Discontinuous Shear Thickening that is qualitatively similar to measurements of suspensions in standard rheology setups, despite the fact that there is no liquid. Thus, the interstitial liquid is not a necessary component for shear thickening when the grains are confined by other means.

A large hysteresis loop can be seen for  $\phi = 0.625$  in Fig. 19. This is the threshold beyond which – at larger gap sizes, corresponding to lower packing fractions – the measured shear stress was below the resolution limit suggesting contact between the plate and grains was lost. This emphasizes that a key role of the liquid is simply to keep contact with and transmit stress between the particles and the plate. The gap size where contact was lost is the same as where the yield stress vanished, which also requires plate-particle contact.

We repeated these measurements with liquid water filling the measurement volume and surrounding so there was no liquid-air interface near any particles. With water, contact between the suspension and plates could be maintained at larger gaps (lower packing fractions). However, no significant difference was seen in the qualitative aspects of Discontinuous Shear Thickening or in the scale of  $\tau_{max}$  for  $\phi \geq 0.625$  with or without water.

An upper bound on the jamming transition can be identified by the point where the shear stress drops below the measurement resolution, is  $\phi = 0.62$ , confirming

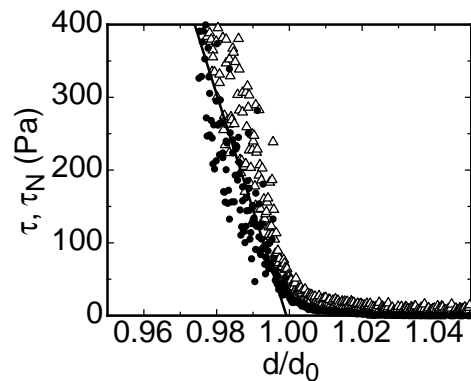


FIG. 20: Shear stress  $\tau$  and normal stress  $\tau_N$  for a sample of 500  $\mu\text{m}$  glass spheres with no liquid under compression with solid walls. The gap  $d$  is normalized by the gap  $d_0$  at the jamming transition for this volume of sample. The sample is compressed at a rate of  $0.25\mu\text{m/s}$  and sheared at a rate of 1 Hz. This is in the range where the shear stress is close to the zero shear rate limit, so the measured  $\tau$  is a good proxy for the yield stress. The solid line is a linear fit used to represent the compressional modulus  $E_s$  of the system of sheared grains and solid wall in series.

that all of the data in Fig. 19 is above the jamming transition. The jamming transition can be at a significantly higher packing fraction dry than with liquid because of the larger density difference between the particles and surrounding fluid [44]. With a solid wall, the yield stress does not plateau at high packing fractions like in the case of a liquid-air interface, but rather increases dramatically as the packing fraction was increased as seen in Fig. 19. This continued up to the maximum stress the rheometer can apply. This can be expected if the confining stress comes from the stiffness of either the wall or particles, in which case the confining stress increases as the solids are further compressed [65]. This is in contrast to the confining stress from surface tension which is limited by a constant scale as packing fraction is increased beyond jamming [22], which is due to the limiting radius of curvature of the liquid-air interface set by the particle size.

To connect  $\tau_{max}$  to a confining stress for closed systems, we made measurements of the compressional modulus of the tool and sample in series. We observed that the rearrangement of particles under shear makes the suspensions much more compliant than under compression alone. Thus we sheared the samples while measuring the compressional modulus to better match the usual experimental conditions. The sample was slowly compressing at a fixed rate of  $0.25\mu\text{m/s}$  while also shearing at fixed rate of 1 Hz (3 mm/s). The shear rate was much faster than the compression rate so that the packing has time to rearrange as it is being compressed, but slow enough that the shear stress is still near the zero shear rate limit as seen in Fig. 19. The measured shear and normal stresses are shown in Fig. 20.

The compressional modulus of this system is calculated as  $E_s = -\partial\tau/\partial(d/d_0)$  where the gap size is normalized by

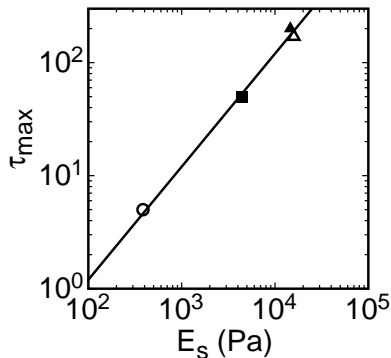


FIG. 21: Maximum stress of the shear thickening regime  $\tau_{max}$  vs. effective boundary modulus  $E_s$  for 600  $\mu\text{m}$  glass spheres under several different boundary conditions. Open circle: standard parallel plate setup, and particles were suspended in water in the so there is a liquid-air interface at the boundary. Solid triangle: hard wall rheometer setup, and particles were suspended in water. Open triangle: hard wall, no liquid. Solid square: hard wall with a soft foam rubber insert, and particles were suspended in water. The solid line corresponds to a strain on the boundary of 0.012, suggesting a volume increase by dilation in the same amount.

a reference gap size  $d_0$ , defined as the point where a linear extrapolation of the stress reaches zero which is shown in Fig. 20. This modulus is much less than the value obtained by compressing the sandpaper by itself, which is the weakest component of the wall. Thus the presence of the grains has a significant effect on the effective modulus, despite the fact that the material modulus is much higher than that of the sandpaper.

We plot values of  $\tau_{max}$  vs. the measured system modulus  $E_s$  in Fig. 21 each for the wet and dry 500  $\mu\text{m}$  glass spheres. We also measured a set of stress/shear curves and compression curves for the wet glass spheres with a layer of soft foam rubber inserted between the top plate and sample as shown in Fig. 1b, and the corresponding values of  $\tau_{max}$  and  $E_s$  are also plotted in Fig. 21. Finally, for comparison to the standard parallel plate measurements with a liquid-air interface, we plot  $\tau_{max}$  vs. an effective modulus taken from Fig. 16 as  $E_s = d/(2\partial\delta/\partial\tau) = 380$  Pa (the factor of 2 is the binomial expansion coefficient of from the change in volume of a cylinder with the radius). It can be seen that each experiment, all of which were done with different boundary conditions, can be described by the linear relationship  $\tau_{max} = 0.01E_s$ . The coefficient can be interpreted as the strain on the boundary, which is equivalent to a normalized dilation  $\delta/d$ . The value on the order of 1% is typical of measurements of dilation of granular packings [43, 44]. This confirms that, for a wide range of boundary conditions with different boundary stiffness, the scale of  $\tau_{max}$  is proportional to the modulus of that boundary which is due restoring force from the dilation of the sample against the boundary under shear.

## XI. DISCUSSION

### A. Dominant stress scales

So far we have described the boundaries of the shear thickening regime  $\tau_{min}$  and  $\tau_{max}$  in terms of dominant stress scales in different parameter regimes. Here we attempt to discuss these stress scales in the most general terms possible to describe a single mechanism that applies to all of the parameter regimes.

First we want to focus on the common feature of all of the onset scaling laws for  $\tau_{min}$ . In a previous work we focused on the effect of a particle attractions from various sources including particle-liquid surface tension and induced attractions from external fields [23]. In each case the attractions resulted in a yield stress. The scale of  $\tau_{min}$  was set by the shear stress required to overcome roughly the two-particle attractive force per cross-sectional area of a particle to shear them apart. In contrast, we found that suspensions of particles large enough to settle the scale of  $\tau_{min}$  is set by gravity rather than attractions (Fig. 5). The shear stress needs to be enough to exceed the weight of a particle per cross-sectional area to overcome friction. The common criterion for the onset of shear thickening in all of these cases is that the applied shear stress must exceed all local stress barriers that are responsible for holding the particles in place. Once this threshold is exceeded, local shearing between grains can occur (Fig. 6), which leads to dilation and increased confining stresses resulting in shear thickening.

In cases where interparticle attractions are dominant they also tend to set the scale of the yield stress [23]. Just above the yield stress, the confining stress can start to grow as shear causes dilation, but there must be at least a small shear thinning regime before the confining stress becomes dominant and shear thickening is seen. Indeed, Ref. [1] found the onset of dilatancy at slightly lower shear rates than the onset of shear thickening. In other words, the viscosity minimum corresponds to a transition in the dominance of different stress and not necessarily where the mechanism for shear thickening first appears. In a crossover the viscosity minimum typically occurs when the shear thickening component of the stress exceeds other components which is typically on the scale of the onset of dilation but the precise difference depends on the details of the scaling functions [23, 34].

With this picture we can now try to understand the case of colloids in which the particles have a repulsive electrostatic potential. While attractive particles may have to be pulled apart to shear, repulsive particles may have to be pushed around each other to shear. If the particles push against each other they end up pushing against all of the confining stresses, whose net response is still determined by the softest component of the system. This means we expect the onset stress to be set by the scale of the two-particle interaction stress scale regardless of whether it is attractive or repulsive. Maranzano & Wagner measured  $\tau_{min}$  for repul-

sive (charge-stabilized) colloidal particles from 80 to 700 nm in diameter and known zeta potentials [11]. They fit a scaling for the onset stress of shear thickening to be  $\tau_{min} \propto a^{-2.11 \pm 0.16}$  [11]. The two-particle repulsive force over the cross-sectional area of a particle gives a stress scale of  $16\epsilon\epsilon_0\psi^2/a^2$  for liquid dielectric constant  $\epsilon$  and electrostatic potential  $\psi$ . This has both the same scaling and magnitude within about a factor of 2 of the data, consistent with the idea that the onset of shear thickening is set by the repulsive stress scale. The same scaling was argued for by Hoffman [70]. This onset scaling is consistent with the general criterion that the applied shear stress must exceed the local stress barrier that is responsible for holding particles in place. The idea that it does not matter whether the interparticle potential is attractive or repulsive is familiar in jammed systems. For example, gels can form due to either attractions or repulsive interactions. In simulations of jammed systems it has been shown that the shape or sign of the potential is not relevant to whether the system will jam, but the magnitude of the potential does set the scale of the global moduli in either case [65].

The regime that has received the most attention theoretically is the Brownian-motion dominated regime. In this regime the onset of shear thickening is usually expressed in terms of a critical Peclet number  $Pe_c = kT/\eta\dot{\gamma}a^3$  [36]. This has been found to describe the onset of shear thickening in Brownian-dominated systems when rewritten in terms of a critical stress scale of  $\tau_{min} = kT/6\pi a^3$  [12, 34]. This scale is the osmotic pressure, which is an effective repulsive stress. This Peclet number scaling for the onset works both for Discontinuous and Continuous Shear Thickening [12, 34]. We suggest this is because the scalings for  $\tau_{min}$  are set by mechanisms for shear thinning which are independent of the mechanisms for shear thickening. Either type of shear thickening can be hidden until the stresses from shear thickening mechanisms exceed all stresses from shear thinning mechanisms [23]. This argument is simply based on which stresses are dominant, and so is not specific to particular mechanism or to whether the shear thickening is Discontinuous or Continuous.

Each of the scaling laws for  $\tau_{min}$  correspond to different dominant parameter regimes. To delineate a typical parameter regime for Discontinuous Shear Thickening in suspensions, we show each of the scalings mentioned for bounds of the shear thickening regime in Fig. 22. Since no single suspension has been used to cover the entire parameter space, we give scalings for a hypothetical suspension with some typical material properties, but note that each of the phase boundaries can be tuned independently depending on particle and liquid properties.

As can be seen in Fig. 22, the stress scales for Brownian motion and electrostatic interactions tend to dominant for smaller particles, while the stress scale for gravity is dominant for larger particles. This should not be surprising, as the colloid regime is typically characterized by the importance of Brownian motion, zeta potential,

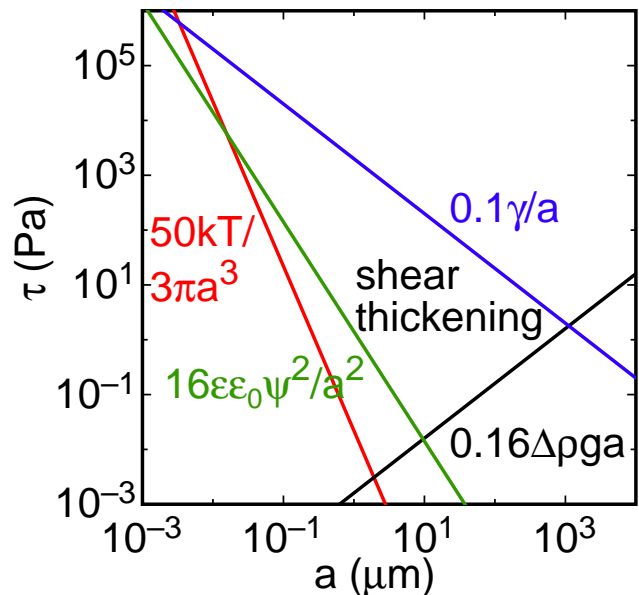


FIG. 22: A rheological state diagram for a hypothetical typical suspension including all known scaling laws for shear thickening regime boundaries. It is assumed the suspension has a liquid-air interface at the boundary and the liquid wets the particles. Red line: Peclet number scaling due to Brownian motion taken from Refs. [13, 34]. Green line: Electrostatic repulsion scaling based on Ref. [11] for a surface potential  $\psi = 70$  mV. Blue line: confining stress from surface tension with  $\gamma = 20$  mN/m. Black line: gravitational scaling with a density mismatch  $\Delta\rho = 1$  g/mL. Since each boundary depends on different parameters, they can be tuned independently.

or van der Waals forces, while the suspension regime is characterized by the importance of gravity. These scales meet at some intermediate size, which could be used to define the colloid-suspension transition. Depending on the values of zeta potential, density, and so on, the scalings for  $\tau_{min}$  typically meet around  $10 \mu\text{m}$ . This suggests that suspensions of particles on this size scale will tend to have the smallest values of  $\tau_{min}$ , which is roughly in agreement with Fig. 5. This suggests an optimal particle size for shear thickening where the largest stress range for the shear thickening regime will typically be found.

The maximum particle size at which shear thickening was found was about  $1000 \mu\text{m}$  (Fig. 5). An upper bound is expected when  $\tau_{min} \sim \Delta\rho ga$  which is set by gravity and increases with particle size meets with  $\tau_{max} \sim \gamma/a$  which is set by surface tension and decreases with particle size, as seen in Fig. 22. This corresponds to a microscopic capillary length scale  $a \sim \sqrt{\gamma/(\Delta\rho g)}$  which differs from the usual capillary length in two ways. First, this microscopic capillary length depends on the density difference rather than just a liquid density. Second, this microscopic capillary length sets a transition between scaling regimes based on particle size rather than system size. This means surface tension effects can be seen in sus-

pensions on much larger scales than would usually be expected based on the macroscopic capillary length. The microscopic capillary length should typically be around  $1000 \mu\text{m}$  for most suspensions, in agreement with the maximum size particle found to shear thicken. While this gives a typical particle size scale above which most particles will not shear thicken in suspension, it is less tied to this size scale than the macroscopic capillary length because it depends on the density difference, as the maximum particle size could in principle be much higher for density matched suspensions.

The minimum particle size is not well known, as most measurements have been done for particles larger than  $0.1 \mu\text{m}$ . The scalings in Fig. 22 suggest the Brownian and surface tension scalings cross at around  $0.004 \mu\text{m}$ , but there are other factors to consider. It is also predicted that the particle modulus may become a limiting factor when the confining stress from other sources becomes large [35]. If any other particle interaction scales exceed the confining stress from surface tension, we would expect shear thinning mechanisms to be dominant over shear thickening [23]. We have left some such particle interactions out of the state diagram because the corresponding scaling laws for  $\tau_{min}$  are not established. These interactions include hydrogen bonding [68], depletion [34], or a particle-liquid surface tension [5, 23]. The rarity of observations of shear thickening in dense suspensions and colloids can in part be explained by the fact that many colloids fall into this regime where the stress scale of particle interactions from some source exceeds the confining stress scale so they do not have any shear thickening regime. Another likely reason for the apparent rarity of shear thickening is that it occurs in a fairly small parameter space with a narrow range in packing fraction, so many measurements of suspension rheology simply do not cover this range.

It is notable that cornstarch, the most famous shear thickening particle, is on the optimal size scale of around  $10 \mu\text{m}$ . In terms of chemical properties, cornstarch we have found it notable only in that it is extremely hygroscopic which implies minimal particle-liquid surface tension and consequent shear thinning effects in water [23], which also happens to have one of the highest surface tensions of typical liquids. Cornstarch remains an inert, hard particle in aqueous suspension, in contrast with some other mass-produced powders such as flour which gel in water at room temperature. Thus we attribute the strong shear thickening of cornstarch to its optimal particle size, and lack of the various interactions which produce shear thinning effects in other suspensions.

So far we have given stress scales for typical suspensions which implies a particle size range where shear thickening is usually expected. However, in most cases these were not fundamental limits and one could do better with engineered suspensions. The maximum particle size of  $a \sim \sqrt{\gamma/(\Delta\rho g)}$  suggests shear thickening could be found for much larger particles if they were density matched. If a strong shear thickening response is de-

sired, then a high surface tension with small particles is suggested. If shear thickening is not desired, reducing the packing fraction or using softer particles (which could include a soft potential) are straightforward options. Many engineered suspensions are stabilized to prevent settling by some interparticle interaction. If the stress scale of the stabilizing interaction is larger than the confining stress scale, the stabilization may also have the effect of hiding shear thickening.

## B. Confining stress in other systems

In this section we consider the confining stress scale for different types of granular systems and what that says about why they do or do not shear thicken.

We found the upper bound of the shear thickening regime  $\tau_{max}$  to be set by the confining stress which comes from the restoring force when grains dilate against a boundary, either from surface tension when there is a liquid-air interface (Figs. 17, 18) or by the stiffness of the wall when all boundaries are solid (Fig. 21). In the discussions of the confining stress so far, the most compliant boundary always set the response. This is because the stiffness of a system of several elements with very different stiffnesses in series will generally be determined by the most compliant element in the series. In some systems, the particles could be the most compliant element. This regime would be relevant when all of the walls are very hard, and it has been proposed such a regime may be reached for small colloidal particles where the confining stress from surface tension is larger [35]. If there is a lubrication layer of liquid between gaps, the maximum confining stress would be coupled to the viscosity because the particle compression depends on the stress in the lubrication layer. For solid contacts between elastic spheres, the confining stress would scale as  $(\delta/R)^{3/2}E_p$  where  $E_p$  is the compressional modulus of the particles and  $\delta/R$  corresponds to the compressional strain on the sample. The  $3/2$  power comes from the contact between two spherical surfaces as opposed to the power of 1 for flat surfaces. For the hard particles we used with  $E_p \sim 10^{10}$  and  $\delta \approx 10^{-2}$ , this confining stress is of order  $10^7$ , which is much stiffer than the liquid-air interface.

Dry grains in an open container are not known to shear thicken. When they shear they dilate but there is no interface to provide a restoring force so there is no confining stress. It is clear now that the important difference between dry and wet grains is that the surface tension of the liquid provides a confining stress. It is only when we provide a confining stress by enclosing the system with solid walls that shear thickening can be found for dry grains (Fig. 19). This emphasizes the fact that not only is dilation required for shear thickening, but also that it must be partially frustrated by a restoring force from the boundary, otherwise there is no confining stress.

Some measurements of sheared dense suspensions found only inertial scaling rather than Discontinuous

Shear Thickening [28]. Notably, those experiments were done in an enclosed system but with a rubber sheet in the wall to allow dilation of the suspensions and a liquid reservoir. Thus it seems likely that the rubber sheet was soft enough that its compression did not provide a significant confining stress in excess of the inertial contribution to the stress. In other words, if the enclosure is very compliant allows dilation without producing a confining stress, then we expect similar behavior to an open system. This suggests a possible method for reducing the resistance in pipe flow of dense suspensions would be to use compliant walls and a liquid reservoir.

A closed system with very hard walls is expected to cause the grains to jam as there is no room for dilation and the hard walls would be able to apply enough stress to hold particles in place. This effect has been seen for hard disks in a hard-walled system just below the onset of jamming based on uniform compression. The disks contacted each other via force chains when sheared quasi-statically, i.e. the system jammed rather than shear thickened [72]. Alternately, plug flow with slip at the walls may also be allowed, but this would not shear thicken either. In contrast to the case for suspensions with a liquid-air interface, the yield stress above the jamming transition with hard walls scales with the particle modulus as the particles compress against each other, which is the most compliant component of the system if the walls are harder. This results in a different scaling for the yield stress with packing fraction, since with hard walls the confining stress increases as the system is further compressed to higher packing fractions [65], while for a suspension the confining stress is limited by the scale  $\gamma/a$  regardless of further compression.

Foams are another system used for jamming experiments with soft particles. Rheologically they are generally found to shear thin, even in confined volumes. Since bubbles are very soft, they will be the limiting factor that determines the confining stress, which will be very low. It seems unlikely that the confining stress can exceed attractive interactions considering they both come from surface tension, so shear thickening should not be expected.

Molecular liquids are classic Newtonian fluids, yet on a molecular level they are a disorganized collection of particles. While molecular liquids can exhibit an apparent shear thickening due to inertial effects at high Reynolds numbers, they do not generally exhibit Discontinuous Shear Thickening. In slow unidirectional shear flows of molecular liquids there are no normal forces. This implies liquid molecules in bulk can shear past each other without dilation or confining stresses, and thus Discontinuous Shear Thickening should not be expected.

An important feature that makes granular materials distinct from molecular liquids and foams is that only the hard grains dilate under shear. This dilation leads to a stress determined by the boundary condition and shear thickening. Soft or otherwise unconfined particles can shear without a significant confining stress which can

result in a Newtonian rheology if the particles are not strongly interacting. If particle interactions are dominant, shear thinning is usually found. Only confined hard particles can dilate against a confining stress to result in shear thickening.

Most simulations of suspension have so far failed to produce Discontinuous Shear Thickening [29, 33, 36, 41, 47, 49, 50]. These simulations have included viscous interactions as well as various interparticle interactions. Most have focused on bulk behavior, usually using periodic boundary conditions such as Lees-Edwards to avoid dealing with boundary effects. Now that we have recognized that the boundary conditions and especially the confining stress are important to shear thickening, it seems likely that many of these simulations did not find Discontinuous Shear Thickening because of the boundary conditions. The one simulation that has produced Discontinuous Shear Thickening was a molecular dynamics simulation of 2-dimensional granular shear flow with frictional contacts between particles but no liquid or viscous interactions [55]. Besides a steep  $\tau(\dot{\gamma})$  at packing fractions just below the jamming transition, quantitatively they found the scale of the normal and shear stresses was set by the particle modulus, which in that simulation was the only scale that could set a confining stress. This may be a minimal model for Discontinuous Shear Thickening in 2 dimensions since it includes particle-particle contacts with a restoring force, but leaves out the liquid.

### C. Connection to solid mechanics

We showed that the scale of the large stress response of shear thickening is set by a confining stress. A close analogy can be made to other systems, for example in the field of soil mechanics. In typical soil mechanics tests, a granular material is compressed or sheared under some known applied confining pressure. The confining pressure on a soil determines the scale of the stress response against shear or compression [73]. An important distinction is that soil mechanics tests are generally done with a controlled fixed confining stress, so there is no shear thickening transition.

One lesson to take away from soil mechanics is that even though the global response of the system is set by the boundary, the scale of the stress response is not dependent on sample size or shape. This is because forces will transmit throughout the bulk across particle contacts, and forces must balance across the system, regardless of how far across the bulk is. This makes stress the appropriate size-independent force scale as in other continuum systems. In Discontinuous Shear Thickening suspensions, the same qualitative behavior has been seen in as few as 2 particle layers [24] to tens of thousands of layers [11]. Quantitatively, the significance of the surface area to volume ratio can be checked by varying the gap size in a parallel plate geometry for a fixed volume of sample because the surface area changes. For such

measurements at constant shear rate, it was found that the percentage change in stress was  $(0.20 \pm 0.22)\%$  over a range where the surface area changed by 17% for a gap size range from 0.71 to 1 mm where other finite size effects were negligible [24]. This is consistent with a shear stress independent of surface area and inconsistent with a stress proportional to surface area. Similar results have also been found when comparing Couette cell measurements with parallel plate measurements [21]. These observations support the argument that the relevant stress scale for shear thickening is not dependent on the system size or shape.

It has been suggested that shear thickening is a form of jamming [11, 21, 36, 39, 71]. Visible shear in and above the shear thickening regime shows that shear thickening is not jamming in the strict sense of yield stress or even static structures. In this sense it seems more correct to characterize the shear thickening transition as unjamming. Below the onset of shear thickening, the particles may be settled or stuck together by attractions; in either case this corresponds to a locally static structure, and in many cases the system is truly jammed with a yield stress below the shear thickening regime. The shear thickening regime is where more of the particles becomes involved in shear, causing increased dilation against the boundaries which cases the shear stress to increase dramatically (Fig. 6).

One connection between Discontinuous Shear Thickening and jamming comes from the observation that they are controlled by the same critical packing fraction  $\phi_c$  [22]. The shear rate at the onset of shear thickening goes to zero in the limit of  $\phi_c$ , suggesting the limiting case of shear thickening corresponds to a yield stress, i.e. a jammed state, which is also what is found on the other side of  $\phi_c$  [22]. The other connection between Discontinuous Shear Thickening and jamming comes from the observation that the scale of the stress response of each is controlled by a confining stress which is transmitted via force chains, which was hinted at by Refs. [59, 60]. Thus Discontinuous Shear Thickening could be considered to be a dynamic extension of jamming, but so far there is not yet a formalism for describing jamming in non-static systems.

#### D. Summary of the mechanism for shear thickening

Here we briefly summarize the results which explain the proposed mechanism for Discontinuous Shear Thickening in suspensions. Shear thickening begins when the shear stress overcomes stresses holding the grains together and they start to shear relative to each other (Figs. 5, 6). This shear between grains causes the grain packing to dilate (Figs. 14, 15). Dilation causes the particles to push against a compliant boundary, typically the liquid-air interface for suspensions open to the air, which pushes back with a restoring force to produce a confining stress on the suspension (Figs. 16, 17, 18). The result-

ing normal stresses are transmitted through the packing through frictional interactions (Figs. 8, 9, 10,11), resulting in a rapid increase in shear stress with shear rate.

Based on this mechanism, the requirements for Discontinuous Shear Thickening, not necessarily limited to suspensions, can be stated as:

1. Dilation: The system must dilate when sheared. This usually requires a high packing fraction, close to the jamming transition.
2. Confining stress: There must be a confining stress that provides a strain-dependent restoring force against dilation. This confining stress can come from surface tension at a liquid-air interface, the walls surrounding the system, or the particle stiffness.
3. Dominance of confining stress: The confining stress must exceed all stresses that prevent granular shear and dilation, such as interparticle interactions or gravity. Otherwise, the confining stress does not provide enough stress increase to result in a positive slope on a viscosity curve and the global rheology may be shear thinning instead.

Hoffman [4] argued that Discontinuous Shear Thickening will occur in dense suspensions whenever the particles segregate into layers but are constrained from rotating as groups below the onset stress. While Wagner showed that the layering is not necessary [13, 17, 19], we are in agreement that the onset is determined by a point where the shear stress is large enough to shear particles in such a way to cause dilation. The shear thickening described by Hoffman with an order-disorder transition seems to satisfy the conditions we set here.

Many other papers have supported a hydrocluster mechanism [11, 18, 33] based on the ability of those models to predict some of the onset scalings shown in Fig. 22. We have argued that these onset scalings can be more simply understood in terms of dominant stress scales which are more general and not dependent on a base hydrodynamic model. Specifically, we have generally seen scalings corresponding to a frictional stress transfer rather than a viscous stress transfer (Fig. 10).

We found that the local bulk viscosity obtained from shear profile measurements corresponded to shear thinning (Fig. 9), even for a global mechanical response that corresponded to shear thickening. This apparent contradiction can now be explained to be due to the change in the boundary condition with dilation which has a dominant effect on the global response, but which is not characterized by the local bulk viscosity. This would imply that under a definition based on local bulk viscosities, those suspensions were not shear thickening. Considering the mechanism we have proposed seems generally able to explain observations of Discontinuous Shear Thickening, it seems possible that none of the observations corresponded to a discontinuous shear thickening in a local constitutive sense. We have continued to use the

term Discontinuous Shear Thickening not only because the term is common in the literature, but also because it describes a universal phenomenon that has a dramatic effect on the global mechanical response of dense suspensions.

### E. Remaining problems

We have been able to determine the mechanism for Discontinuous Shear Thickening and approximately how the stress boundaries depend on suspension parameters. However, many details remain unresolved. For example, the slope of viscosity curves in the shear thickening regime should depend on how dilation depends on shear rate or stress and packing fraction, but this is not well-understood in suspensions. Dilation in suspensions at non-zero shear rates occurs at packing fractions significant lower than for dry grains in the quasi-static limit [44, 66, 74]. This suggests hydrodynamic models may still be useful for understanding dilation in suspensions. As an example, simulations have shown that a pair of particles compressed together by viscous forces can rotate in the plane of the shear gradient together which should cause the structure to dilate [51].

It is often desirable to describe rheology in terms of constitutive laws so general field equations can be written for flows in different geometries. While we have shown that the momentum transfer equation is dominated by a simple frictional law (Fig. 10), a set of constraints including the boundary conditions is also required. A particular challenge from this point of view is that this would have to include dilation which drives inhomogeneities and changes the boundary conditions.

We have been able to quantify connections between shear thickening and jamming in terms of a critical packing fraction as well as stress scales set by a confining stress. This suggests that it would be useful to develop a framework for jamming that goes beyond the static case to apply to granular shear flows.

## XII. ACKNOWLEDGEMENTS

We thank S. Nagel, T. Witten, and W. Zhang for thoughtful discussions. We thank Marc Miskin for designing the optical setup used in the  $\text{ZrO}_2$  and polyethylene videos. We thank Franco Tapia Uribe for taking preliminary shear profile measurements. We thank Trevor Martin for machining the solid wall setup for the rheometer. This work was supported by DARPA through Army grant W911NF-08-1-0209 and by the NSF MRSEC program under DMR-0820054.

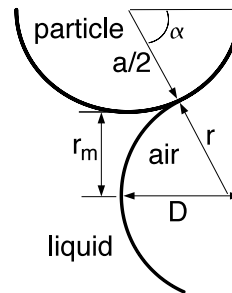


FIG. 23: Dimensions used for calculation of relationship between dilation  $\delta$  and confining stress due to surface tension at an interface with radius of curvature  $r$ .

## XIII. APPENDIX: CALCULATION OF CONFINING STRESS AT LIQUID-AIR INTERFACE FROM DILATION

To connect the confining stress at the liquid-air interface to the measured dilation  $\delta$  a model is needed for the interface geometry. For simplicity we will assume spherical particles with a contact angle  $\theta = 0$  at the liquid-solid-air contact line since to obtain shear thickening the liquid must wet the particles. For this contact angle the interface geometry is equivalent to a sphere of air of radius  $r$  in contact with particles at the surface. We will calculate the geometry for a characteristic radius of curvature as if it is the same at each interstice between particles, and use these mean single-particle calculations an estimate for the surface as a whole, ignoring variations in the surface curvature. The point of contact is defined by an angle  $\alpha$  relative to horizontal as shown in Fig. 23. The packing fraction of particles on the two dimensional surface will be represented by  $\phi_{2D}$ . As an estimate we will use the value  $\phi_{2D} = 0.84$  which corresponds to random close packing in two dimensions [75]. This geometry gives enough constraints to relate the radius of curvature  $r$  to the contact angle to obtain a confining stress from surface tension. The dilation  $\delta$  can be connected to this geometry and thus the confining stress by using conservation of volume.

From the geometry in Fig. 23, the vertical components of the dimensions can be used to relate the radius of curvature to the contact angle

$$r \sin \alpha = \frac{a}{2}(1 - \sin \alpha) + r_m . \quad (8)$$

The minimum radius of curvature  $r_m$  comes from the minimum radius of the interstitial gap between particles. At an interstice between 3 particles in contact, this is  $r_m/a = \sqrt{1/3} - 1/2 \approx 0.26$  in three dimensions, but in two dimensions  $r_m$  would be zero. The mean confining stress is modeled as

$$\tau_{conf} = \frac{\gamma}{r}(1 - \phi_{2D} \sin^2 \alpha) \quad (9)$$

where  $1 - \phi_{2D} \sin^2 \alpha$  is the fractional cross-sectional area around the outer edge covered by the liquid-air interface.

To relate the dilation  $\delta$  to the contact angle, conservation of volume provides the necessary constraint. The volume of air per particle in the region up to the maximum particle extent can be represented by

$$\Delta V = 2V_{cap} + V_{int} \quad (10)$$

where  $V_{cap}$  is the volume of a spherical cap interior to the point of contact (of which there are 2 per particle)

$$V_{cap} = \frac{\pi r^3}{3} (1 - \cos \alpha)^2 (2 + \cos \alpha) \quad (11)$$

and  $V_i$  comes from integrating the fluid volume in the mean surface normal direction from the furthest point of penetration of the particle up to the point of contact:

$$\begin{aligned} V_i &= \int_0^\alpha \frac{\pi a^3}{4} \sin \alpha' \left[ \frac{1}{\phi_{2D}} - \sin^2 \alpha' \right] d\alpha' \\ &= \frac{\pi a^3}{4} \left[ \frac{1 - \cos \alpha}{\phi_{2D}} - \frac{\cos(3\alpha) - 9 \cos \alpha + 8}{12} \right]. \end{aligned} \quad (12)$$

Conservation of volume requires that the dilation match the enclosed volume of air per particle up to the maximum penetration of the particle

$$\delta = \frac{4\phi_{2D}\Delta V(r, \alpha)}{\pi a^2}. \quad (13)$$

Since  $\delta$  and  $\tau_{conf}$  are both functions of  $r$  and  $\alpha$ , they can be related by numerically solving Eqns. 8, 9, and 13, with the result shown in Fig. 16.

These equations may be valid until the point where the contact line reaches the 2nd layer of particles from the surface, beyond which extra contact lines are made. This starts when the maximum penetration  $D = (a/2 + r)(1 - \cos \alpha)$  reaches  $\sqrt{3}a/2$  which corresponds to the layer width for a hexagonal packing. This limit is shown as the dashed line in Fig. 16.

- 
- [1] A. B. Metzner and M. Whitlock, *Trans. Soc. Rheol.* **11**, 239 (1958).
- [2] R. L. Hoffmann, *Trans. Soc. Rheol.* **16**, 155 (1972).
- [3] R. L. Hoffmann, *J. Colloid Interface Sci.* **46** 491 (1974).
- [4] R.L. Hoffmann. *Advances in Colloid and Interface Sci.* **17** 161 (1982).
- [5] H.A. Barnes, *J. Rheology* **33** (2), 329 (1989).
- [6] W.H. Boersma, J. Laven, H.N. Stein, *AIChE* **36**, 321 (1990).
- [7] H.M. Laun, *J. Non-Newtonian Fluid Mech* **54** 87 (1994).
- [8] W.J. Frith, P. d'Haene, R. Buscall, J. Mewis, *J. Rheology* **40**(4), 531 (1996).
- [9] J. Bender, N. Wagner, *J. Rheology* **40** (5), 899 (1996).
- [10] V.T. O'Brien and M.E. Mackay, *Langmuir* **16**, 7931 (2000).
- [11] B. J. Maranzano and N. J. Wagner, *J. Chem. Phys.* **114**(23), 10514 (2001).
- [12] B. J. Maranzano and N. J. Wagner, *J. Rheol.* **45**(5), 1205 (2001).
- [13] B. J. Maranzano and N. J. Wagner, *J. Chem. Phys.* **117**(22), 10291 (2002).
- [14] E. Bertrand, J. Bibette, and Véronique Schmitt, *Phys. Rev. E* **66**, 060401(R) (2002).
- [15] D. Lootens, H. Van Damme, and P. Hébraud, *Phys. Rev. Lett.* **90**, No. 17, 178301 (2003).
- [16] D. Lootens, H. van Damme, Y. Hémar, and P. Hébraud, *Phys. Rev. Lett.* **95**, 268302 (2005).
- [17] R.G. Egres and N. J. Wagner, *J. Rheol.* **49** (3), 719 (2005).
- [18] S. S. Shenoy and N.J. Wagner, *Rheol. Acta.* **44**, 360 (2005).
- [19] R. G. Egres, F. Nettekheim, and N.J. Wagner, *J. Rheol.* **50**(5), 685 (2006).
- [20] Y.S. Lee and N.J. Wagner, *Ind. Eng. Chem. Res.* **45**, 7015 (2006).
- [21] A. Fall, N. Huang, F. Bertrand, G. Ovarlez, and D. Bonn, *Phys. Rev. Lett.* **100**, 018301 (2008).
- [22] E. Brown and H.M. Jaeger, *Phys. Rev. Lett* **103** 086001 (2009).
- [23] E. Brown, N. A. Forman, C. S. Orellana, H. Zhang, B. W. Maynor, D. E. Betts, J. M. DeSimone, and H. M. Jaeger, *Nature: Materials* **9** (3) 220-224 (2010).
- [24] E. Brown, H. Zhang, N. A. Forman, B. W. Maynor, D. E. Betts, J. M. DeSimone, and H. M. Jaeger, *J. Rheol.* *accepted arXiv:0912.0529* (2010).
- [25] Y.S. Lee, E.D. Wetzel, and N.J. Wagner, *J. Materials Sci.* **38**, 2825 (2003).
- [26] S.S. Shenoy, N.J. Wagner, and J.W. Bender, *Rheol Acta* **42**, 287 (2003).
- [27] M.R. Jolly, and J.W. Bender, US patent application No. 20060231357.
- [28] R.A. Bagnold, *Proc. Royal Soc. London A: Math. and Phys. Sci.* **225**(1160), 49 (1954).
- [29] J. Bergenholtz, J.F. Brady, and M. Vucic, *J. Fluid Mech.* **456**, 239 (2002).
- [30] C.O. Osuji, C. Kim, and D. A. Weitz, *Phys. Rev. E* **77**, 060402 (2008).
- [31] R.J. Larsen, J.-W. Kim, C. F. Zukoski, and D.A. Weitz, submitted to *Phys. Rev. E* (2010).
- [32] A. Fall, A. Lemaître, F. Bertrand, D. Bonn, G. Ovarlez, submitted to *Phys. Rev. Lett.* (2010).
- [33] J. Brady, G. Bossis. *J. Fluid Mech.* **155**, 105 (1985).
- [34] V. Gopalakrishnan and C.F. Zukoski, *J. Rheol.* **48**(6), 1321 (2004).

- [35] J.F. Brady, N.J. Wagner, *Phys. Today*, Oct. 2009, 27.
- [36] R.S. Farr, J.R. Melrose, and R.C. Ball, *Phys. Rev. E* **55**(6), 7203 (1997).
- [37] H.M. Jaeger, S.R. Nagel, R.P. Behringer, *Rev. Mod. Phys.* **68**, 1259 (1996).
- [38] A.J. Liu and S. R. Nagel, *Nature* **396**, 21 (1998).
- [39] M.E. Cates, J.P. Wittmer, J.-P. Bouchaud, and P. Claudin, *Phys. Rev. Lett.* **81**, (9) 1841 (1998).
- [40] T.S. Majmudar and R.P. Behringer, *Nature* **435**, 1079 (2005).
- [41] J. R. Melrose, R. C. Ball, *J. Rheology* **48**(5), 961 (2004).
- [42] D.M. Mueth, G.F. Debregeas, G.S. Karczmar, P.J. Eng, S.R. Nagel, and H.M. Jaeger, *Nature* **406**, 385 (2000).
- [43] O. Reynolds, *Phil. Mag.* **20**, 469 (1885).
- [44] G. Y. Onoda and E. G. Liniger, *Phys. Rev. Lett.* **64**(22), 2727 (1990).
- [45] A. Fall, F. Bertrand, G. Ovarlez, and D. Bonn, *Phys. Rev. Lett.* **103**, 178301 (2009).
- [46] A.I. Jomha and P.A. Reynolds, *Rheol. Acta* **32** 457 (1993).
- [47] J.R. Melrose, J.H. van Vliet, and R.C. Ball, *Phys. Rev. Lett.* **77**(22), 4660 (1996).
- [48] A. Sierou and J.F. Brady, *J. Rheol.* **46**(5), 1031 (2002).
- [49] J.R. Melrose and R.C. Ball, *J. Rheol.* **48** (5), 937 (2004).
- [50] D. S. Grebenkov, M.P. Ciamarra, M. Nicodemi, and A. Coniglio, *Phys. Rev. Lett.* **100**, 078001 (2008).
- [51] D.I. Dratler, W.R. Schowalter, and R.L. Hoffman, *J. Fluid Mech.* **353**, 1 (1997).
- [52] A.J. Goldman, R.G. Cox, and H. Brenner, *Chem. Eng. Sci.* **22**, 652 (1967).
- [53] R.J. Donnelly and N.J. Simon, *J. Fluid. Mech.* **7**, 401 (1960).
- [54] L. Bocquet, W. Losert, D. Schalk, T.C. Lubensky, and J.P. Gollub, *Phys. Rev. E* **65**, 011307 (2001).
- [55] M. Otsuki, H. Hayakawa, arXiv:1006.3597 (2010).
- [56] J. F. Brady and M. Vicic, *J. Rheol.* **39**(3), 545 (1995).
- [57] M.I. Smith, R. Besseling, M.E. Cates, and V. Bertola, submitted to ? (2010).
- [58] J.B. Knight, C.G. Fandrich, C.N. Lau, H.M. Jaeger, and S.R. Nagel, *Phys. Rev. E* **51**(5), 3957 (1995).
- [59] C.B. Holmes, M. Fuchs, and M.E. Cates, *Europhys. Lett.* **63** (2), 240 (2003).
- [60] C.B. Holmes, M. E. Cates, M. Fuchs, and P. Sollich, *J. Rheol.* **49**(1), 237 (2005).
- [61] M.E. Cates, R. Adhikari, and K. Stratford, *J. Phys.: Condens. Matter* **17**, S2771 (2005).
- [62] D.A. Weitz, J.P. Stokes, R.C. Ball, and A.P. Kushnick, *Phys. Rev. Lett.* **59**(26), 2967 (1987).
- [63] W.H. Boersma, P.J. M. Baets, J. Laven, and H.N. Stein, *J. Rheol.* **35**(6), 1093 (1991).
- [64] Z. Janssen, *Verein Deutsch. Ing.* **39**, 1045 (1895).
- [65] C. S. O'Hern, L. E. Silbert, A. J. Liu, and S.R. Nagel, *Phys. Rev. E* **68**(1), 011306 (2003).
- [66] M. Jerkins, M. Schröter, H. L. Swinney, T. J. Senden, M. Saadatfar, and T. Aste, *Phys. Rev. Lett.* **101**, 018301 (2008).
- [67] V. Trappe, V. Prasad, L. Cipelletti, P.N. Segre, and D.A. Weitz, *Nature* **411** 772 (2001).
- [68] S.R. Raghavan, H.J. Walls, and S.A. Khan, *Langmuir* **16**, 7920 (2000).
- [69] W. Gallay and I.E. Puddington, *Can. J. Res. C* **21**, 179 (1943).
- [70] R.L. Hoffman, *J. Rheol.* **42**(1), 111 (1998).
- [71] P. Hébraud and D. Lootens, *Mod. Phys. Lett. B* **19**(13-14), 613 (2005).
- [72] J. Zhang, T. Majmudar, and R. Behringer, *Chaos* **18**, 041107 (2008).
- [73] T.W. Lambe and R.V. Whitman, (1969) *Soil Mechanics* (John Wiley and Sons, New York).
- [74] A.J. Kabla and T.J. Senden, *Phys. Rev. Lett.* **102**, 228301 (2009).
- [75] C.S. O'Hern, S.A. Langer, A.J. Liu, and S.R. Nagel, *Phys. Rev. Lett.* **88**(7), 075507 (2002).
- [76] In some of the literature a distinction is made between discontinuous and continuous shear thickening at different packing fractions based solely on the slope of the viscosity curve. However, in many cases there is no qualitative change in behavior or identifiable transition in scaling when the packing fraction is varied. Thus we do not follow this convention because it does not suggest different phenomena.
- [77] For  $\phi_m \gtrsim 0.4$ ,  $\eta_m$  is likely an overestimate of the viscous contribution to viscosity as the non-Newtonian terms become larger near the jamming transition and  $\eta_m$  likely just represents a cross-over between the shear thinning and shear thickening effects [23]. Regardless, since the viscous contribution to the viscosity increases while the onset shear rate decreases with packing fraction, the onset Reynolds number still becomes very low at high packing fractions.
- [78] Ref. [21] performed similar measurements. They also found that the shear and normal stress dropped significantly after a short transient peak. This showed that there was a connection between the shear and normal stress in the transient behavior, and they suggested that the shear thickening disappeared without the normal force after this transient behavior. However, the scale of the peak stress shown was about  $10^5$  Pa, so high that the stress they measured in steady state shear thickening also would have appeared to be zero on that scale. Even if the stress drops down significantly, a viscosity curve is needed to determine whether or not there is shear thickening.